공학박사 학위논문

Mechanistic Study and Development of a Catalyst for Glycerol Conversion to Acrolein

글리세롤 탈수반응의 반응기작 연구와 안정적인 촉매 개발

2017년 2월

서울대학교 대학원

화학생물공학부

윤 다 님

Abstract

Mechanistic study and development of a catalyst for glycerol conversion to acrolein

Danim Yun
School of Chemical and Biological Engineering
The Graduate School
Seoul National University

Since the demand for a clean and green technology has increased, countless efforts have been made to replace conventional petrochemical processing. Biomass could be a solution to satisfy the needs of the times because it has a potential for producing fine chemicals or building blocks without increasing greenhouse gas emissions. Therefore, various studies concerning the production of value-added chemicals from biobased compounds have been reported in recent years. In particular, the conversion of glycerol to acrolein has attracted a considerable amount of attention as an alternative route to the production of acrolein from petroleum-based propylene. Furthermore, an increasing cost ratio of acrolein to glycerol in recent years makes the conversion also economically viable. In this thesis, catalytic mechanism for glycerol dehydration via Brønsted acid site is studied, and a sustainable catalyst for acrolein production is developed.

At first, the catalytic mechanism of glycerol dehydration on Brønsted acidic amorphous aluminosilicate is explored via first principle calculation. Si-(OH)-Al groups of amorphous aluminosilicate have been known to play important

roles in acid catalyzed reactions. However, there is a lack of theoretical understanding on the catalytic function of the acid sites and reaction mechanisms on the amorphous aluminosilicate surface. Here, the preferred glycerol dehydration mechanism on Si-(OH)-Al sites was investigated. It was found that when the primary OH group of glycerol is adsorbed on Brønsted proton (Si-(OH)-Al sites), the adsorption strength is too strong to convert to acetol. On the other hand, the secondary OH group of glycerol is adsorbed with a relatively moderate strength at the acid site, which then leads to favorable production of 3-hydroxypropionaldehyde (3-HPA). Consequently, the 3-HPA is readily dehydrated into acrolein and water due to its reactive properties. Therefore, glycerol is preferentially converted into acrolein on amorphous aluminosilicate during dehydration. In order to verify the preferential formation of acrolein, catalytic activity test was experimentally conducted. The amorphous aluminosilicate catalyst exhibited remarkable selectivity for acrolein (39.8%), which supported our theoretical approach. In addition, the adsorbed and polymerized glycerol on the used catalyst surface was identified via ^{13}C NMR. This suggests that when glycerol is too strongly adsorbed, it can be transformed into coke during dehydration. Combining our theoretical and experimental observations, it was concluded that strongly adsorbed glycerol gives rise to not only a lower level of conversion to acetol, but also coke deposition on the amorphous aluminosilicate surface.

Then, a catalyst for the sustainable conversion of glycerol to acrolein is designed and investigated. Developing a catalyst to resolve deactivation caused from coke is a primary challenge in the dehydration of glycerol to acrolein. An open-macropore-structured and Brønsted-acidic catalyst (Marigold-like silica functionalized with sulfonic acid groups, MS-FS) was synthesized for the stable and selective production of acrolein from glycerol. A high acrolein yield of 73% was achieved and maintained for 50 h in the presence of the MS-FS catalyst. The hierarchical structure of the catalyst with

macropores was found to have an important effect on the stability of the catalyst because coke polymerization and pore blocking caused by coke deposition were inhibited. In addition, the behavior of 3-hydroxypropionaldehyde (3-HPA) during the sequential dehydration was studied using density functional theory (DFT) calculations because 3-HPA conversion is one of the main causes for coke formation. We found that the easily reproducible Brønsted acid sites in MS-FS permit the selective and stable production of acrolein. This is because the reactive intermediate (3-HPA) is readily adsorbed on the regenerated acid sites, which is essential for the selective production of acrolein during the sequential dehydration. The regeneration ability of the acid sites is related not only to the selective production of acrolein but also to the retardation of catalyst deactivation by suppressing the formation of coke precursors originating from 3-HPA degradation.

Keywords: Glycerol dehydration, acrolein, a sustainable catalyst, reaction mechanism

Student Number: 2011-21051

Contents

List of Tables

List of Figures

List of Schemes

Chapter 1. Introduction

1.1 Glycerol as an by-product of biodiesel production

Development of renewable liquid fuels and chemicals has been significant interest due to environmental, economic, and political motivation. In order to efficiently manage the greenhouse gas emissions, dependence on petroleum has to be reduced, and biomass conversion can be one of the solutions. Biomass is biological material, and it can be used as a sustainable carbon source. When using biomass, we could produce bioenergy and biochemical, and this can replace the fossil-based chemical processes [1].

Bioenergy usually indicates biofuels, which consist of biodiesel and bioethanol. The bioethanol is mainly produced by fermentation of starch, and biodiesel is formed from triblycerides by transesterification reaction using alkali catalysts. Glycerol is a by-product of the transesterification process. 100 kg glycerol is produced when treating 1 ton of biodiesel [2]. The production of biodiesel is increased rapidly and is even forecasted to increase to 36.9 million metric tons in 2020 [3] and the produced amount of glycerol will be also increased.

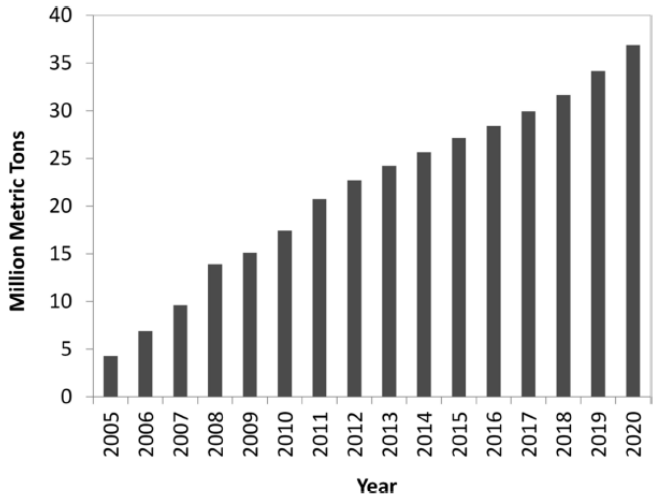

Figure 1-1. Annual production of biodiesel. Figure is reprinted from [3]

1.2 Dehydration of gas-phase glycerol over acid catalysts

Various catalytic reaction, such as steam reforming, oxidation, dehydration, acetalization, esterification, etherification, carbonxylation, and chlorination, can be procceded to produce useful chemicals from glycerol (Figure 1-2) [4]. Among these vaious utilizations, the dehydration of glycerol into acrolein has been intensively investigated [5-7], because the acrolein is considerably useful building block. Acrolein can be used to form acrylic acid, acrylic acid esters, superabsorber polymers, and detergents.

The general glycerol dehydration network is presented in Figure 1-3. The product distribution in glycerol dehydration depends on which OH group of glycerol is abstracted first [8-10]. When the primary hydroxyl group of glycerol is dehydrated, acetol and water are produced. Acetol is relatively stable; thus, it is a main by-product of gas-phase dehydration. On the other hand, when the secondary hydroxyl group of glycerol is detached as a water molecule, 3-hydroxypropionaldehyde (3-HPA) and water are formed. 3-HPA has reactive property, which is attributed to the carbonyl group [11]. It could be converted to form stable conjugation of C=O and C=C bonds. In this case, reactive 3-HPA is readily dehydrated on acid sites into water and acrolein.

One of the most interesting aspects of the catalytic process of glycerol dehydration is that selectivity is dependent on the acid types of the catalysts [8, 12]. In the fist dehydration step in glycerol conversion, Brønsted acid sites are

more effective to produce acrolein than Lewis acid sites [8-10, 13]. For example, the amorphous aluminosilicates are one of strong Brønsted acid catalysts, thus, they shows high selectivity for acrolein from glycerol. However, the study of catalytic mechanism on Brønsted acid sites is insufficient, because the observation of intermediate (3-HPA) using experimental is limited, due to the unstable property of it. Therefore, the catalytic mechanism is needed to be explored using density functional theory (DFT) calculation.

On the other hand, glycerol conversion to acrolein can be procceded under both liquid phase and gas phase condition. In addition, acrolein can be obtained using subcritical and supercritical water or homogeneous catalysts [14-16]. Dehydration of gas-phase glycerol has been more intensively studied because the acrolein yields were the highest under the gas phase condition. In the case of gas-phase reaction, however, the secondary reactions of glycerol cracking can occur, which leads to the severe coke formation. Although high acrolein selectivity has been reported over solid acid catalysts in many reports [5-7], the catalysts are deactivated rapidly in most cases and the development of a catalyst which shows sustainable production of acrolein from glycerol is still required.

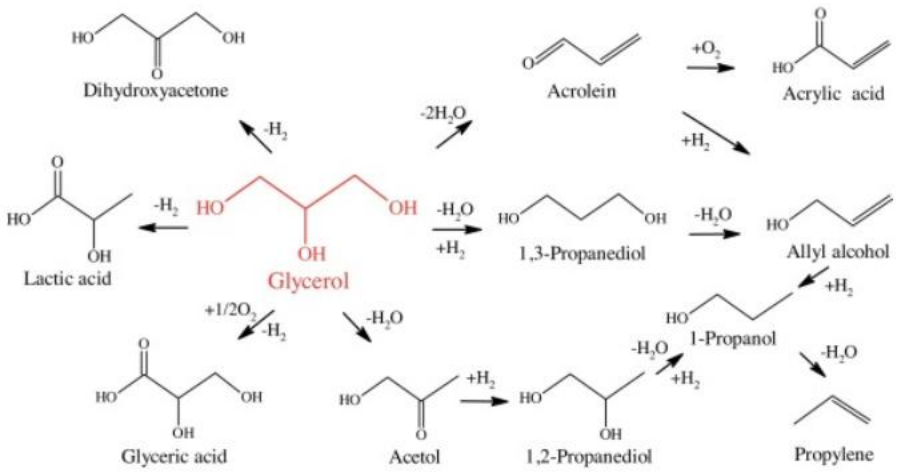

Figure 1-2. Glycerol conversion into various chemicals. Figure is reprinted from [4]

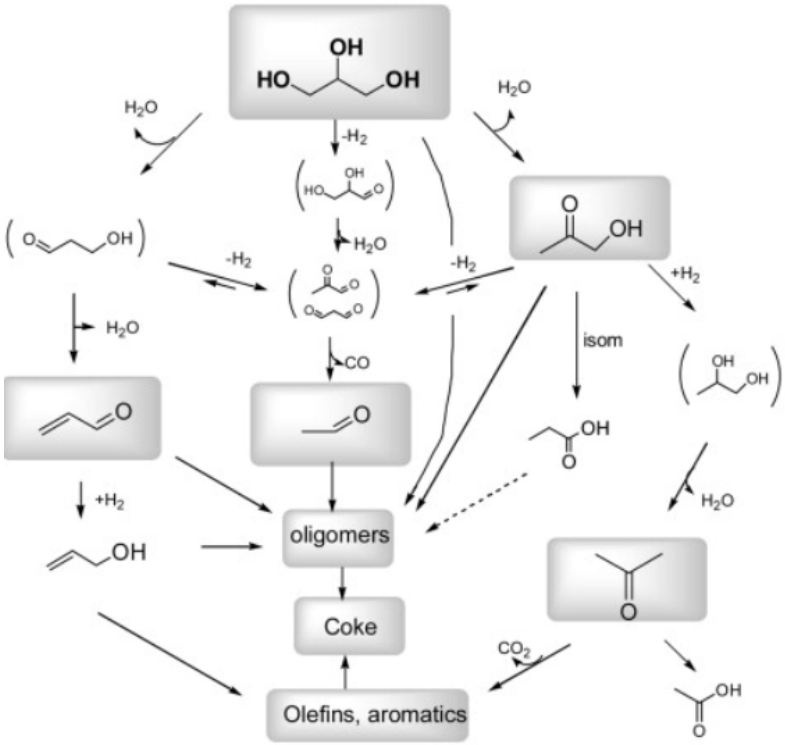

Figure 1-3. General glycerol conversion scheme. Reactant and main products have been highlighted. Figure is reprinted from [9]

1.3 Objectives

In this thesis, catalytic mechanism for glycerol dehydration on Brønsted acid sites of amorphous aluminosilicate is investigated via density functional theory calculation. The surface of amorphous aluminosilicate is constructed and adsorption and activation energies of each elemental step is calculated. Based on these calculation results, the preferred catalytic mechanism over Brønsted acid site of amorphous aluminosilicate was suggested. Then, the expected mechanism was verified via experimental results.

A novel catalyst for sustainable production of acrolein from glycerol is developed. The catalyst is designed considering the coke deposition during glycerol dehydration. The reason why developed catalyst shows the remarkable productivity for a long time is also discussed based on the mecahnistc perspective.

Chapter 2. Mechanistic study of glycerol dehydration on Brønsted acidic amorphous aluminosilicate

2.1 Introduction

Since amorphous aluminosilicate was recognized as a highly active acid catalyst, many efforts have been made to reveal the relationship between the chemical structure of acid sites and catalytic activity [18–21]. In particular, the chemical structure of acid sites on amorphous silica-alumina (ASA) has been debated for decades. Crépeau et al. [22] have proposed silanol groups near Lewis acid Al^{3+} sites as Brønsted acid sites of ASA. Williams et al. [23] have reported that the water molecules bonded to surface Al atoms are responsible for the acidity of ASA. According to their models, acidity of ASA would be expected to show moderate acidity. However, Poduval et al. [24] revealed that ASA possesses acid sites with strong acid strength as well as moderate one. Except for Si-(OH)-Al group, others such as silanol groups near Lewis acid Al3+ sites or water molecules bonded to surface Al atoms could not be the strong acid sites in ASA. In addition, pseudo-bridging silanols have been pointed as major components to cause acidity of ASA, theoretically [20] and experimentally [25]. The chemical structure of acid sites on ASA cannot be clearly explained yet. However, Si-(OH)-Al groups

have attracted attention in various acid catalytic reactions in that they are strong Brønsted acid sites [19] and enable the production of value-added chemicals from hydrocarbons [26–28].

Despite the significant role of Si-(OH)-Al groups, there has been an insufficient amount of theoretical investigation into the catalytic function of Si-(OH)-Al groups in amorphous aluminosilicate. This is because realization of an amorphous structure by means of periodic density functional theory (DFT) calculation is somewhat challenging. However, recent progress in modeling a structure of amorphous silica using b-cristobalite crystals [29] has made it possible to obtain various amorphous metal oxide structures. For example, functionalized-silica [30], mixed oxide [31] and supported oxide [32, 33] catalysts were developed using a b-cristobalite model, which allowed their catalytic properties in the reaction to be investigated via theoretical calculation.

Aluminosilicates show superior selectivity for acrolein in the glycerol dehydration because they have abundant Brønsted acid sites on the surface [7]. According to a previous report [34], the Brønsted acidity of aluminosilicate is strongly affected by neighboring Al atoms. When the Al content of aluminosilicate is increased, the ratio of Brønsted to Lewis acid strength is increased. This means that the Si-(OH)-Al groups of aluminosilicate can play a crucial role in glycerol dehydration as a selectivity-determining factor. However, how glycerol is converted on Si-(OH)-Al sites of aluminosilicate has not been studied. To achieve this, theoretical study is mandatory because it is difficult to comprehensively

understand complex catalytic mechanisms based solely on experimental results. Moreover, observation of unstable intermediates (3-HPA) during glycerol dehydration is generally not available via experimental methods.

In the present study, the surface structure of amorphous aluminosilicate was developed using a β-cristobalite model, and the catalytic mechanism of glycerol dehydration on Si-(OH)-Al sites was investigated via DFT calculation. The adsorption structures and activation energies for each step of glycerol dehydration at Si-(OH)-Al sites are presented. In addition, theoretical expectations are verified via experimental results, whereby the predicted selectivity for each product is compared with the outcome from catalytic activity test, and deposited carbon species of the used catalyst is confirmed to demonstrate the suggested reaction pathway. The calculated adsorption energy, proposed catalytic process and coking in the use of aluminosilicate were compared to those in the use of H-ZSM-5 based on the previously reported results.

2.2 Methods

2.2.1 Comptational methods

All calculations were carried out using a Vienna ab initio simulation package (VASP, version 5.3.2) [35]. The generalized gradient approximation (GGA) parameterized by a Perdew-Burke-Ernzenhof (PBE) exchange-correlation functional [36] was employed and core electrons were represented by the projector-augmented wave (PAW) method [37]. Dispersion forces were taken into account with the DFT-D2 Grimme's empirical correction [38]. An energy cutoff for the plane waves of 400 eV was applied. The geometry optimizations were performed using a 3 × 3 × 1 Monkhorst−Pack mesh for the k-point sampling. The total energies were converged until the forces on all atoms were less than 0.03 eV/Å. The electronic optimization steps were converged self-consistently to $<2 \times 10^{-4}$ eV.

An amorphous aluminosilicate surface was constructed using a β-cristobalite (111) surface [39]. The β-cristobalite structure was used to represent amorphous silica due to similar properties such as its refractive index and bulk density [40-42]. On the developed silica surface, the Si atom was replaced by an Al atom with a constant molar ratio (Si/Al=15) in its bulk structure. In our calculations, all atomic positions were fully relaxed and the surface consisted of Si slabs of 4 layers with ~20 Å of vacuum space. In order to determine the number of Si layer, we constructed amorphous aluminosilicate surface with 6 Si layers, and the adsorption energies of

glycerol via different OH group were calculated. As a result, adsorption configurations and energies were very similar in spite of the increase in the number of slab. This indicates that 4 Si layers are enough to establish the aluminosilicate surface. Bader charge analysis [43] was performed to evaluate the charge redistribution on silanol and Si-(OH)-Al groups.

Gas-phase glycerol was used based on previous study results, which showed it to be one of the stable conformers [44]. In their results, the molecular energies and structures of 126 possible conformers were presented. We selected the 5 most stable configurations based on their results, and then determined which was the most stable.

The adsorption energies for single molecules were calculated as follows:

$$\Delta E_{ads} = E_{adsorbate/surface} - E_{adsorbate} - E_{surface}$$

The co-adsorption energies for the product with a water molecule were calculated as follows:

$$\Delta E_{co\text{-}ads} = E_{(adsorbate+H2O)/surface} - E_{adsorbate} - E_{H2O} - E_{surface}$$

Deprotonation energy was calculated based on a reaction with gaseous water molecule ($H_A + H_2O(g) \leftrightarrow A^- + H_3O^+(g)$), and following equation for deprotonation energy was used:

$$E_{DPE} = E_{A-} + E_{H3O+,gas} - E_{HA} - E_{H2O,gas}$$

where H_A and A^- represent the acid site and deprotonated acid site, respectively.

The charge density difference (Δq_i) was defined as follows:

$$\Delta q_i = q_{i,after\ adsorption} - q_i - q_{surface}$$

where $q_{i,\text{after adsorption}}$, q_i and $q_{surface}$ denote the charge density of the adsorbed system, molecule i and the surface, respectively.

Activation energy barriers and the transition images for all elementary steps were calculated using the climbing-image nudged elastic band (CI-NEB) method [45, 46]. At least five intermediate images were interpolated between reactant and product states. In the CI-NEB calculations, the images were sampled using a 1 × 1 × 1 Monkhorst-Pack k-point grid and obtained until the maximum atomic forces were converged within 0.05 eV/Å. When harmonic frequencies were calculated for NEB-optimized transition states, only a single imaginary frequency was obtained in all cases. We calculated activation energies for the first dehydration step from various adsorption modes including less stable ones, and then we found the lowest activation energy for each step.

In order to figure out the preference of adsorbed glycerol to be desorbed form the catalyst surface, the adsorption equilibrium constant and the free energy of the adsorption were calculated using the following equations.

$$\Delta G_{ads} = -RT\ln K_{ads}$$

$$\Delta G_{ads} = \Delta H_{ads} - T\Delta S_{ads} \approx E_{Total} - (E_{surface} + E_{glycerol}) + T(S^{rotational}_{glycerol} + S^{translational}_{glycerol})$$

where E_{total}, $E_{surface}$, and $E_{glycerol}$ are DFT calculated energies, and $S^{rotational}_{glycerol}$ and $S^{translational}_{glycerol}$ are rotational and translational entropy of a gas-phase glycerol. The entropy values were obtained from the cluster-based DFT calculation (Gaussian 03, B3LYP functional, 6-311G basis set).

2.2.2 Catalyst preparation

Amorphous aluminosilicate nanosphere, denoted as ASN, was prepared via our previously reported method [47]. Briefly, 1 g of cetylpyridinium bromide hydrate and 0.6 g of urea were dissolved in deionized water (30 mL). Then, 2.5 g of tetraethyl orthosilicate and 1.5mL of 1-pentanol were added in cyclohexane (30 mL). The prepared two solutions were mixed and stirred for 30 min at 25 ^{o}C. The mixture was hydrothermally treated with continuous stirring at 120 ^{o}C for 2.5 h in an autoclave. After cooling to room temperature, pH was controlled to 5 by adding HCl solution (2 M). Then, an $Al_2(SO_4)_3 \cdot 18H_2O$ solution (0.204 M, 2 mL) was added, and the resultant solution was hydrothermally treated again at 120 ^{o}C for 4 h. The product was centrifuged and washed three times with a solution of acetone and water. Then, the collected sample was dried at room temperature for 24 h and calcined in air at 550 ^{o}C for 6 h. HZSM-5 was obtained after the calcination of commercial zeolite NH_4ZSM-5 (Si/Al=15, Zeolyst, product No. CBV 3024E) at 550 ^{o}C for 6 h.

2.2.3 Catalytic activity test

The dehydration of glycerol was carried out under atmospheric pressure at 300 ^{o}C. To begin, 5 mg of catalyst was loaded into a quartz reactor (8 mm inner diameter) and pre-treated at 300 ^{o}C for 1 h under a flow of N_2 (30 $mL \cdot min^{-1}$). 1.2 M glycerol solution was fed into the reactor by a syringe pump at a rate of 2.0 $mL \cdot h^{-1}$. The temperature of inlet line was 270 ^{o}C to

vaporize the glycerol solution and the gas hourly space velocity (GHSV) was 843.2 $L \cdot g_{catalyst}^{-1} \cdot h^{-1}$. After the glycerol dehydration, the products were passed through a condenser, and then collected in a cold trap. The collected products were analyzed via a gas chromatograph (Younglin ACME 6500 model) equipped with a FID detector and a HP-Innowax capillary column. Glycerol conversion and product selectivity were calculated as follows:

$$\text{Glycerol conversion (\%)} = \frac{\text{mole of glycerol reacted}}{\text{mole of glycerol fed}} \times 100$$

$$\text{Yield (\%)} = \frac{\text{mole of product}}{\text{mole of glycerol fed}} \times \frac{C_i}{3} \times 100$$

$$\text{Selectivity (\%)} = \frac{\text{mole of product}}{\text{mole of glycerol reacted}} \times \frac{C_i}{3} \times 100$$

where C_i represents the number of carbon atoms of product i.

Carbon balance was calculated by summing the unreacted glycerol and the total amount of detected products.

2.2.4 Characterization

The amount of coke deposited on the catalyst was determined by CHNS analysis (Flash1112, CE Instrument).

The acid amount and strength of the catalysts were evaluated by the temperature-programmed desorption (TPD) of NH_3. 0.1 g of a sample was loaded in a quartz reactor and preheated at 200 °C for 2 h under a He flow (20 $mL \cdot min^{-1}$). After cooling to 50 ^oC, the sample was treated under a flow of 10% NH_3/He (20 $mL \cdot min^{-1}$) for 1 h. The physisorbed NH_3 was eliminated

by He flow (50 mL·min^{-1}) at 50 ^{o}C for 1 h, and the chemisorbed NH_3 was quantitatively detected using a Micromeritics Autochem II chemisorption analyzer with an on-line mass spectrometer (QGA, HIDEN ANALYTICAL). In this step, temperature was increased from 50 ^{o}C to 700 ^{o}C under a He flow (50 mL·min^{-1}).

In order to analyze property of cokes, catalytic activity test was performed using 0.05 g of catalyst. The used catalyst was collected after the glycerol dehydration for 5 h. Solid-state ^{13}C CP-MAS NMR data were collected on an AVANCE 400 WB spectrometer. The samples were placed inside a 4 mm rotor and were rotated at 7 kHz MAS speed. For the ^{13}C CP-MAS measurements, the pulse sequence was a frequency of 100.7 MHz and a spectral width of 31 kHz. The cp4c.35 (cross-polarization MAS) pulse program and a relaxation delay of 5 s were used. The ^{13}C chemical shifts were referenced relative to Glycine.

2.3 Adsorption of glycerol molecule on amorphous aluminosilicate surface

2.3.1 Construction of the amorphous aluminosilicate surface

In general, it is difficult to create models of amorphous materials for DFT calculation due to a lack of periodicity. However, in the case of amorphous silicate, it was possible to describe the characteristics via the use of a β-cristobalite structure that is known to resemble the physicochemical properties of amorphous silicate. In previous theoretical studies [40-42], amorphous silica-based catalysts were employed via the use of β-cristobalite SiO_2, which successfully captured the experimental trends. In this regard, we used a β-cristobalite structure as the framework for amorphous aluminosilicate.

Aluminosilicate can be synthesized via various experimental methods that include physical mixing [48], a two-step process [49] a microwave-hydrothermal route [50], and a binary surfactant system [51]. Among the various synthetic methods, post-grafting is widely used because it eases the building of active sites on the surface of a catalyst. When aluminosilicate is synthesized via post-grafting method with silica template, most of the Al atoms are located on the surface of the silica.

C. Chizallet et al. [20] first reported the amorphous aluminosilicate surface model by simulating the contact of silica derivatives with the γ-Al_2O_3 (100) surface. They also provided experimental evidence that the developed surface would be realistic. It should be noted that in their work an amorphous

aluminosilicate phase was formed upon thermal treatment of grafted silica on γ-Al_2O_3 (100). This model, however, cannot be representative for all case of amorphous aluminosilicate. Especially, aluminosilicate synthesized by post-grafting method with amorphous silica template cannot be applied in the previous model. Therefore, we tried to construct another model of amorphous aluminosilicate which consists of amorphous silica framework and Al species as a grafting unit.

We previously reported a post-grafting preparation, referred to as "pH-assisted delay addition", to synthesize amorphous aluminosilicate [47]. After finishing this synthetic process, Al MAS NMR confirmed that most of the Al species were tetrahedrally coordinated in the framework, implying that the Al atoms were successfully introduced onto the surface of the amorphous silica. The crystal structure of the prepared aluminosilicate was amorphous and the molar ratio of Si to Al was 15~60. Based on these experimental demonstrations, an amorphous aluminosilicate surface similar to the existing catalyst (represented by β-cristobalite SiO_2) was developed using DFT calculations. First, the surface of amorphous silica, as referred to by X. Rozanska et al. [39], was constructed, followed by the substitution of Al atoms to Si atoms on the surface. The molar ratio of Si to Al was patterned after the experimental compound (Si/Al=15). Then, OH groups were functionalized between Si and Al atoms in order to create strong Brønsted acid sites. In other words, H atom was put on the bridging oxygen (Si-O-Al) of the Al substituted β-cristobalite (111) surface, and the surface was relaxed for optimization. To confirm the acid strength of each proton on the

developed surface, Bader charge analysis and deprotonation energy (E_{DPE}) were calculated. The calculated atomic charge of the protons represents how easily an O-H bond dissociates heterolytically [52]. There are four silanol groups and one Si-(OH)-Al group per each surface unit cell (Table 2-1). Among the four silanol groups, however, silanol3 interacts with silanol4 by hydrogen bonding. The properties of interacting vicinal silanol groups differ from those of isolated silanol groups [53], and, therefore, silanol3 and 4 were not considered as control groups. The calculated atomic charges and E_{DPE} of silanol1, silanol2 and Si-(OH)-Al groups are presented in Table 2-1. In the Si-(OH)-Al group, q_H is slightly larger than the other O-H groups, which suggests that the Si-(OH)-Al group is the stronger Brønsted acid site [52]. The deprotonation energy of Si-(OH)-Al group is the smallest among surface protons, which also supports that acidity of Si-(OH)-Al is the strongest.

2.3.2 Conformational structure of a glycerol molecule

Glycerol has various conformations in the gas phase. C. S. Callam et al. reported a low-energy conformer among the 126 possible conformations of glycerol [44]. The 5 most stable conformers were selected based on their calculation results, and the most stable one among them was utilized for further calculations. As shown in Figure 2-1(a), two intramolecular hydrogen bonds ($O2\cdots H_{31}$ and $O1\cdots H_{21}$) can be identified in the isolated glycerol molecule. The lengths of a hydrogen bond are 2.10~2.20 Å and hydrogen bonding angles are 112.3° (O3-H_{31}-O2) and 117.4° (O2-H_{21}-O1), respectively.

The backbone conformation of the gaseous glycerol is identified as αγ (Figure 2-1(b)), which is consistent with the experimental studies [54].

2.3.3 Adsorption modes of the glycerol molecule

In consideration of the adsorption modes, either the primary or the secondary OH group of glycerol can be adsorbed onto a Si-(OH)-Al group via hydrogen bonding. Therefore, the possible adsorption structures for each case were calculated to determine the most favorable ones, and the optimized geometries are shown in Figure 2-2. In the case of adsorption via the primary OH group (hereafter referred to as, ads_primary), a glycerol molecule forms six hydrogen bonds with the surface. As shown in Figure 2-2(b), the primary hydroxyl group points to a Si-(OH)-Al group with an O1⋯HA distance of 1.38 Å. This hydroxyl group also heads for a silanol group on the surface, and the hydrogen bonding length is 1.71 Å (Figure 2-2(a)). Other hydroxyl groups of glycerol also points to the silanol groups of aluminosilicate, where the distances of the hydrogen bonds are 1.79~2.01 Å. In H-bonded solids, the hydrogen bond interval between 1.2 and 1.5 Å means that bond strength is quite strong [55]. Therefore, the calculated bond length reveals that glycerol is strongly interacted with the Brønsted acidic sites (Si-(OH)-Al groups), but that it is formed much weaker contacts with the silanol groups. This trend is also confirmed via a charge-density-difference plot (Figure 2-3(a)). A densely concentrated charge density indicates that bond character is covalent, while a distributed charge density implies that the bond is close to ionic [56]. Figure 2-3(a) confirms that the charge density between the Si-(OH)-Al group

and the OH group of glycerol is very concentrated. On the other hand, there are less accumulation of charge density and less depletion between the silanol groups and the OH group of glycerol. This demonstrates a stronger level of hydrogen bonding is formed between the Si-(OH)-Al group and glycerol.

In contrast, when the secondary OH group is adsorbed (ads_secondary), only 5 hydrogen bonds are formed. Similar to ads_primary, the hydroxyl groups of glycerol bind to silanol and to the Si-(OH)-Al group at the aluminosilicate surface. The secondary OH group is in contact with the surface, and points to the Brønsted proton ($O2\cdots H_A$: 1.51 Å, Figure 2-2(d)) to form a strong hydrogen bond. The secondary hydroxyl group also points to a silanol group at a distance of 1.95 Å (Figure 2-2(c)). The remaining hydroxyl groups are bound with the silanol groups (1.73~1.84 Å), leading to additional stabilization after adsorption by the weak hydrogen bonds. The charge density differences in ads_secondary were also calculated (Figure 2-3(b)). The charge density is largely concentrated between the Brønsted acid site and the OH group of glycerol. This supports that the glycerol is adsorbed onto the Brønsted acid site of the amorphous aluminosilicate surface as a result of strong hydrogen bonding.

As a consequence of the differences in the number of hydrogen bonds and lengths, the adsorption energy for ads_primary (E = -1.91 eV) is higher than that of the ads_secondary (E = -1.52 eV). This indicates that the adsorption of the primary OH group of glycerol onto the Si-(OH)-Al site is both strong and stable. In Figure 2-2(b, d), the hydrogen bond lengths and H_A-O_A

distance are shown. The hydrogen bonding between OH groups and Brønsted protons on the aluminosilicate surface results in a weakening of the H_A-O_A bonds. For the ads_primary, the O1$\cdots H_A$ is the shorter (1.38 Å) than the O2$\cdots H_A$ (1.51 Å) for the ads_secondary. In addition, the length of the H_A-O_A bond is confirmed to be increased to 1.09 and 1.06 Å in the ads_primary and the ads_secondary, respectively, compared with 0.99 Å which is the value of a H_A-O_A bond length on the bare aluminosilicate surface. These results also demonstrate the strong adsorption of the ads_primary.

These calculation results are considerably different from those in the use of H-ZSM-5 catalyst [10]. According to K. Kongpatpanich et al., the adsorption energy for ads_secondary is the lower than that for ads_primary in the initial stage of glycerol dehydration over H-ZSM-5 zeolite. This is different results from our calculation results. Therefore, we found that the adsorption structure and strength can be altered by neighbored silanol groups on aluminosilicate surface, although acid site (Si-(OH)-Al) is similar to zeolite.

During the dehydration of glycerol, water molecule can be generated by various ways. In the case of a Lewis acid catalyst, the primary OH group of glycerol is adsorbed onto a metal site and a proton of the secondary carbon of glycerol approaches a bridging oxygen atom of the surface [8]. Then, the surface is hydrated by the OH and H of glycerol, and a water molecule is produced from the catalyst surface. However, the calculated adsorption structures of glycerol on aluminosilicate suggest that the water molecule formation pathway is different from that in a Lewis acid catalyst. In

aluminosilicate, water production is initiated by the protonation of a Brønsted proton in the Si-(OH)-Al site to an OH group of glycerol. This difference is one of the reasons why selectivity depends on the type of acid that is used in the glycerol dehydration.

2.4 The dehydration of glycerol

The glycerol dehydration mechanism is shown in Scheme 2-1. To identify the activation energies for each dehydration step on Si-(OH)-Al sites, detailed reaction pathways were explored via CI-NEB calculations.

2.4.1 Acetol formation via the primary OH adsorption

In the initial stage of acetol formation, the primary OH group of adsorbed glycerol is protonated via a Brønsted proton of aluminosilicate. This protonation leads to the weakening of the primary C1-O1 bond and promotes the removal of the OH group as a water molecule (blue highlighted remark in Figure 2-4(a), H_1-O1-H_A). After the water molecules are produced, deprotonated acid sites can be regenerated in one of two ways depending on which proton is used as a recovery agent, as described in Scheme 2-2. In Case 1, the deprotonated acid site is regenerated by a secondary OH group. The hydrogen atom attached to the secondary carbon C2 is shifted to a carbocation ($C1^+$), and a C=O bond is formed simultaneously. In Case 2, the proton of the middle carbon C2 is used to recover the deprotonated acid site. Then, the produced enol-form is tautomerized to a keto-form. With a H-

ZSM-5 catalyst, glycerol dehydration to acetol is induced via Case 2 [10, 83]. When one OH group of glycerol is adsorbed onto the acid site of H-ZSM-5, the remaining two OH groups do not form hydrogen bonds with the surface, and could even be headed for a vacuum. Accordingly, the hydrogen atom attached to the secondary carbon C2 is in close proximity to the deprotonated acid site of zeolite, thus, the proton from C2 is more easily recovered than that from the secondary OH group.

In amorphous aluminosilicate, the adsorption structure of glycerol is fairly different from that of zeolite. The three hydroxyl groups point toward the surface with hydrogen bonding, which leads to the acetol production via Case 1 in amorphous aluminosilicate. As shown in Figure 2-4(a), O_A is closer to H_{21} (2.80 Å, Case 1) than O_A is to H_{22} (4.37 Å, Case 2). Thus, it is expected that H_{21} is abstracted to protonate the basic aluminosilicate oxygen (O_{A1}). In addition, bond dissociation (C-H vs. O-H) for alcohols reportedly depends on the existence of the hydrogen bonds of neighbors [58]. C-H bond scission is mainly catalyzed without a hydrogen bond network. However, when alcohol is surrounded by hydrogen bonds, the O-H bond dissociation barrier is lowered and the C-H bond scission is slightly inhibited. In a similar manner, the O-H bond strength of glycerol is expected to be weakened due to the hydrogen bonded silanol groups. This also suggests that proton recovery in amorphous aluminosilicate occurs via Case 1.

Simultaneously, H_{22} migrates from C2 to C1 to neutralize the carbocation ($C1^+$), yielding acetol and water (Figure 2-4(a)). The expected transition state structure is considerably similar with the concerted transition state during

dehydration of propylene glycol over solid-acid catalysts reported by T. D. Courtney et al [59].

The produced acetol and water move to the most stable site, and the optimized structure of stably adsorbed acetol and water molecules (ads_acetol+H_2O, E = -1.71 eV) is shown in Figure 2-4(c). Acetol and water interact with the surface by five and two hydrogen bonds, respectively. In the case of acetol, a carbonyl group and a hydroxyl group are bound to the surface. The bonding distances between the functional groups of glycerol and silanols on the surface are 1.75~2.22 Å. The H_{21}-O2 bond length is the shortest (1.63 Å), which implies that the hydrogen bond is the strongest. Water points to the silanol groups on the surface at distances of 2.06 and 2.11 Å, respectively. These O…H lengths are similar to those in the reference study [60].

2.4.2 Acrolein formation via secondary OH adsorption

2.4.2.1 The first dehydration of glycerol to 3-HPA formation

The process of glycerol dehydration to 3-HPA is similar to the acetol formation process. Water production, the regeneration of the basic oxygen site, and the intermolecular migration of protons to neutralize carbocations occur simultaneously. As shown in Figure 2-4(b), glycerol dehydration to 3-HPA is initiated via the protonation of H_A to the secondary OH group of glycerol. After the secondary hydroxyl group and H_A are abstracted as a water molecule (Blue highlighted remark, H_{21}-O2-H_A), carbocation ($C2^+$)

and basic oxygen site are generated. As mentioned above, there are two ways to recover the deprotonated Brønsted acid site depending on the regenerating agent (Scheme 2-3). It is thought that proton recovery proceeds via Case 1 in amorphous aluminosilicate, unlike a zeolite-based catalyst. If a proton is recovered via Case 2, H_{32} or H_{33} would be transferred to O_{A2} or O_{A3} (H_{32}-O_{A2}: 4.82 Å and H_{33}-O_{A3}: 4.90 Å in Figure 2-4(b)), respectively. By comparison, the distance between H_{31} and O_{A2} is much closer (2.66 Å). In addition, the O-H bond of glycerol can be weakened by hydrogen bonded neighbors (silanol groups) [58]. These lead to proton recovery via Case 1 in amorphous aluminosilicate surface. Simultaneously, H_{32} is transferred from C3 to C2 in order to stabilize the carbocation ($C2^{+}$).

Both 3-HPA and water are stabilized on aluminosilicate surface and the optimized structure is shown in Figure 2-4(d). The adsorption strength for ads_3-HPA+H_2O is less (E = -1.63 eV) than that of ads_acetol+H_2O (E = -1.71 eV). The difference could be attributed to the number of hydrogen bonds between the product and the aluminosilicate surface. The 3-HPA is adsorbed onto the aluminosilicate surface with 4 hydrogen bonds which are one less than that of acetol. The carbonyl and hydroxyl groups of 3-HPA are bound to the aluminosilicate surface, where the distances of the hydrogen bonding have a range of 1.53~2.00 Å. Among those bonds, O3⋯H_{31} seems to be the strongest because its length is the shortest (1.53 Å). A water molecule also bounds with the silanol groups of the aluminosilicate surface with distances of 2.15 and 1.79 Å. The calculated O⋯H lengths in ads_3-HPA+H_2O are similar to those reported in reference study [60].

2.4.2.2 The second dehydration of 3-HPA to acrolein

After the first dehydration of glycerol, either acetol or 3-HPA is formed to a substantial degree. Unlike acetol, the 3-HPA is easily converted to acrolein and water because of its reactive properties. In the present study, we assumed that the water molecule produced after the first dehydration would not be involved in the next dehydration step.

After the first dehydration, 3-HPA and the aluminosilicate surface are rearranged to be a thermodynamically stable structure. The diffusion of hydrogen atoms is known to be accelerated by the presence of water molecules on a metal oxide surface.[61] Therefore, the proton transfer from O_{A2} to O_{A1} on the aluminosilicate surface easily proceeds via an H_3O^+ transition state [62]. The hydroxyl group of 3-HPA (O1-H_{11}) is attracted by a strong Brønsted proton, H_{31}, which produces a stable surface adsorption (Figure 2-5(a)). This results in a strong hydrogen bond between O1 and H_{31} at a distance of 1.42 Å. O1-H_{11} also points toward a silanol group on the surface, and hydrogen bonding (1.70 Å) is generated. The terminal carbonyl group interacts with a silanol group via a hydrogen bond with a distance of 1.82 Å. The charge density difference for ads_3-HPA was also calculated. A concentrated charge density is observed between Si-(OH)-Al and the OH group of 3-HPA, which means that the 3-HPA is adsorbed onto the Si-(OH)-Al site via a strong hydrogen bond. The adsorption energy for 3-HPA (ads_3-HPA) on the surface is -1.47 eV.

Similar to the glycerol dehydration, 3-HPA dehydration is initiated by the protonation of H_{31} to the OH group of 3-HPA. After water molecule is produced, basic oxygen (OA1) can be protonated by either H_{32} or H_{22} (Figure 2-5(b)). When the distances between the two protons and basic oxygen were compared, H_{22} is the closer to basic oxygen (2.44 Å) than H_{32} was (3.84 Å). Based on this result, H_{22} is expected to regenerate basic oxygen. After a series of processes, acrolein and water are produced and stabilized on the aluminosilicate surface by three hydrogen bonds (Figure 2-5(c)). The carbonyl group of acrolein interacts with the silanol group of the surface with a bond length of 1.73 Å. This value agreed well with the distances between carbonyl and silanol groups in a previous report [63]. A water molecule is also bound with two silanol groups at distances of 1.80 and 1.83 Å, which are similar values to those reported previously [63]. The C1-C2 bond distance is 1.35 Å, implying that it is double bond that is generated by the stabilization of the two carbocations ($C1^+$ and $C2^+$). The co-adsorption energy is -1.48 eV.

2.5 The catalytic reaction mechanism

The energetic profile of the glycerol dehydration reaction on aluminosilicate is shown in Figure 2-6. In the process of acrolein production, the activation energy for the second dehydration step (1.45 eV) is lower than that for the first dehydration step (1.54 eV). That implies that the first dehydration is the rate-determining step in acrolein production, which agrees well with previous studies [64-66]. In the first dehydration of glycerol, a

noticeable difference in the activation energies for 3-HPA and acetol productions is identified. It is found that 2.09 eV is needed for the acetol production, while 1.54 eV is required to form 3-HPA from glycerol. It means that 3-HPA production is more favorable than acetol production in the first dehydration on the Si-(OH)-Al sites of amorphous aluminosilicate.

The transition state structures of each dehydration step are also presented in Figure 2-6. In the case of transition state for the dehydration of glycerol into acetol, TS_{ACE}, the C1-O1 bond is elongated from 1.45 to 2.54 Å, and this is initiated by the protonation of H_A to the primary OH group of glycerol. Then, an increase in the H_{21}-O2 bond and a decrease in the H_{21}-O_A distance are observed (from 0.98 to 1.04 Å and from 2.80 to 1.51 Å, respectively), indicating that H_{21} is transferred from the O2 to basic oxygen (O_{A1}) in order to regenerate the deactivated Brønsted acid site. Simultaneously, an intramolecular transfer of a proton (H_{22}) in the glycerol molecule from C2 to C1 is confirmed. Based on this image, it is expected that water formation, the protonation of basic oxygen, and proton transfer all would occur simultaneously.

The transition structure for the dehydration of glycerol into 3-HPA, TS_{HPA}, is very similar to the structure of TS_{ACE}. In the transition state, the C2-O2 bond length is increased from 1.45 to 2.38 Å, which indicates that water production proceeds via the protonation of HA to the secondary OH group. The O3-H_{31} bond is elongated from 0.99 to 1.08 Å, and H31 approaches O_{A2} in order to regenerate the deactivated acid site. The migrating of H_{32} from C3 to C2 is also confirmed.

The transition state structure for the conversion of 3-HPA into acrolein and water is represented by TS_{ACR}. Water formation initiated by the protonation of H_{31} to an OH group of 3-HPA, and regeneration of the basic oxygen of aluminosilicate is observed simultaneously. The C1-O1 bond is increased from 1.45 to 1.84 Å, suggesting a C1-O1 bond cleavage and water formation. H_{31} is abstracted from the aluminosilicate surface, and H_{22} moves closer to the basic oxygen site to regenerate the deprotonate site. These are identified by the increase in the C2-H_{22} bond length (from 1.11 to 1.82 Å) and the decrease in the H_{22}-O_A bond length (from 2.44 to 1.04 Å).

To verify our DFT results, catalytic activity test was performed experimentally. In order to provide the reliable information on catalytic mechanism, we obtained catalytic activity results at low conversion level of glycerol. As shown in Figure 2-8(a), the products consist of acrolein (40 %), Acetol (5.8 %) and acetaldehyde (2.3 %) at a glycerol conversion level of 23 %. Other products were not detected. According to previous studies [10, 66-68], acetaldehyde is formed via the degradation of 3-HPA due to the reactive properties of 3-HPA. If it is assumed that acetaldehyde is produced mainly from 3-HPA degradation, then the selectivity for 3-HPA in the first dehydration would be approximately 42 %. Compared to that the selectivity for acetol was 5.8 %, glycerol dehydration via the primary OH group adsorption was remarkably favored (~7 times) on Si-(OH)-Al sites of amorphous aluminosilicate. This trend agreed well with our DFT results.

The catalyst deactivation caused by coke deposition is often observed in gas-phase glycerol dehydration [69, 70]. The deposited coke on the used

ASN catalyst was analyzed by CHNS. The weight fraction of deposited coke during reaction for 1h was 6.2 wt%. As a result, the carbon balance was 89.4 %. The amount of deposited coke is small (Yield of coke: 1.1 %), because ASN catalyst has moderate Brønsted acid strength. The acidity of two catalysts was analyzed by NH_3-TPD-MS. As shown in Figure 2-7, the total amount of adsorbed NH_3 for HZSM-5 is larger than that for ASN catalyst, and the maximum peak for HZSM-5 is located at higher temperature. It indicates that the acid amount and strength of HZSM-5 is the higher than those of ASN catalyst. In this regard, in the case of HZSM-5, more condensed and heavier carbon species are deposited on the surface, leading drastic deactivation. In contrast, it is expected that relatively mild acidity of ASN retarded rapid condensation reaction (formation of hard coke). In order to reveal the cause of coke deposition in amorphous aluminosilicate, the used catalyst was analyzed via ^{13}C NMR (Figure 2-8(b)). The peak centered at 129 ppm originated from aromatic carbon species [71, 72] On the other hand, the signals at 33 and 19 ppm represented the aliphatic carbon [71, 73] and alkyl carbon compounds that are bound to polyaromatics [74], respectively. These aromatic and aliphatic carbon species are likely produced on the strong acid sites of acid catalysts [75, 76]. Interestingly, two peaks at 64 and 74 ppm were also observed and were assigned to absorbed glycerol or to the polymeric forms of glycerol derived from itself [77, 78]. This revealed the existence of glycerol that was too strongly adsorbed onto the catalyst surface, as predicted from our DFT calculations. According to G. S. Foo et al. [79], coke formation in the glycerol dehydration was observed when more

than a monolayer of glycerol was present. This is because at least two molecules are required to form a monoaromatics via multimolecular reactions. This suggests that adsorption strength of glycerol is an important factor in coke formation of glycerol dehydration. Adsorption of glycerol that is too strong evokes multimolecular reactions (coke formation).

In order to figure out the extent to be desorbed from the surface in the ads_primary case, the free energy of the adsorption was calculated. At the reaction temperature of 300 ^{o}C, the free energy of the adsorption is -25.4 kJ/mol, and the adsorption equilibrium constant (K_{ads}) according to this free energy is 209. This high K_{ads} indicates that desorption of glycerol from the catalyst surface does not easily occur at the reaction condition. As mentioned above, the activation energy for glycerol conversion into acetol is considerably high (2.09 eV), thus conversion of glycerol in ads_primary is also not favorable. Therefore, the adsorbed glycerol (ads_primary) is unfavorable to be converted to products nor to be desorbed from the surface, leading to coke formation.

Our results suggested that the additional bondings via silanol groups on aluminosilicate surface lead to distinction of adsorption energy, reaction process, and coking between H-ZSM-5 and aluminosilicate, despite of the similar active sites (Si-(OH)-Al groups).

Finally, the glycerol dehydration mechanism on amorphous aluminosilicate could be proposed, and is shown in Scheme 2-4. When the glycerol is adsorbed onto amorphous aluminosilicate surface, either the primary or secondary OH group points toward the Si-(OH)-Al sites. The adsorption

mode and strength play crucial roles in determining the selectivity of a product. When glycerol is adsorbed with a primary OH group, the activation energy for acetol and water production is too high. This leads to the low selectivity for acetol in products. Moreover, glycerol that is too strongly adsorbed blocks the active sites and promotes catalyst deactivation. On the other hand, when the glycerol is adsorbed with the secondary OH group, the moderate adsorption strength and proper activation energy for this direction enables the favorable production of 3-HPA. Highly reactive 3-HPA is readily converted into acrolein and water at Brønsted acid sites or degraded into acetaldehyde under the reaction conditions [66]. Acrolein could be converted to 2-propenol via hydrogenation reaction, leading oligomers, olefins, aromatics formation. Aldehydes could be oxidized to acids [66, 80] or converted into oligomers via aldol condensation [81]. Acetol by itself is known as unreactive molecule in the presence of Brønsted acid sites. Accordingly, the possible intermediates to cause coke formation are glycerol, 3-HPA, aldehydes (acetaldehyde and formaldehyde), and acrolein.

Table 2-1. Scheme for the location of Brønsted protons in the unit surface and the charges calculated by Bader charge analysis and E_{DPE} for each proton

Scheme	Proton	Calculated charge			E_{DPE}[a] (eV)
		q_H	q_O	$\lvert q_H - q_O \rvert$	
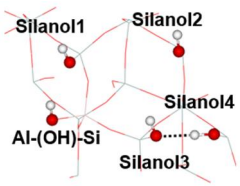	Silanol1	+0.6513	-1.4391	2.0904	8.03
	Silanol2	+0.6796	-1.4582	2.1378	6.28
	Al-(OH)-Si	+0.6861	-1.4753	2.1614	6.18

[a]E_{DPE} was determined by following reaction: $HA + H_2O(g) \leftrightarrow A^- + H_3O^+(g)$, and the protonation energy of water ($E_{PE} = E_{H3O+,gas} - E_{H2O,gas} - E_{H+,gas}$) is 107.46 kcal/mol. VASP employs in the charge neutrality-ensured system due to the periodic boundary conditions. The compensating background charge has to be introduced in the calculations of charged system [82]. This leads to the decrease of the deprotonation energies, therefore, only relative values are meaningful to be discussed.

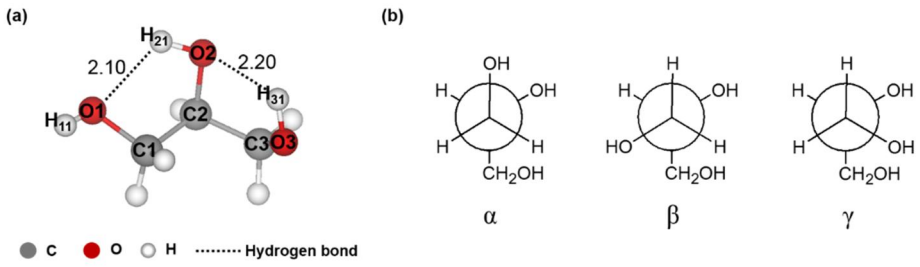

Figure 2-1. (a) The most stable glycerol conformation and (b) possible backbone conformations of glycerol

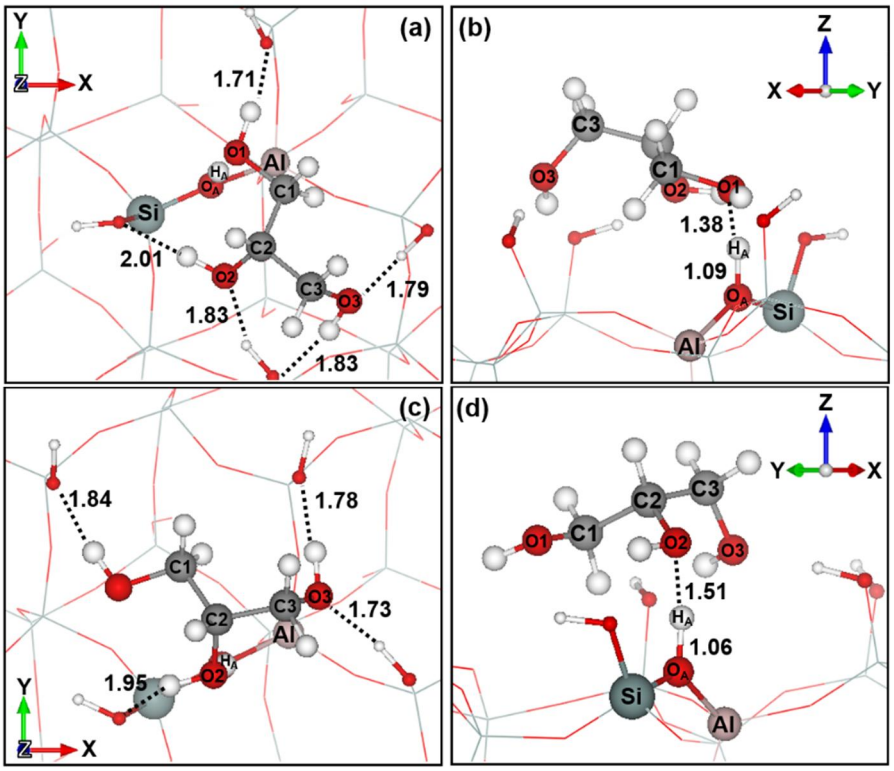

Figure 2-2. (a,c) Top and (b,d) side views of optimized geometries for glycerol adsorption via (a,b) the primary and (c,d) the secondary OH groups of glycerol on Brønsted proton, H_A. The pink, light grey, gray, red, and white spheres (or lines) are for aluminum, silicon, carbon, oxygen, and hydrogen atoms, respectively. The dashed lines indicate hydrogen bonds.

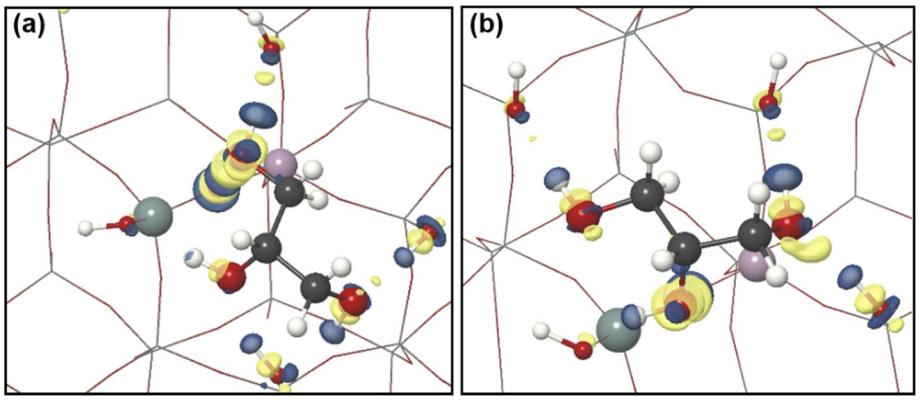

Figure 2-3. The charge density difference plots for hydrogen bonds between surface and the glycerol via the (a) primary and (b) secondary OH groups. Blue color indicates regions of electron accumulation and yellow color indicates regions of electron depletion. Isosurface: 0.006 e/Å^3

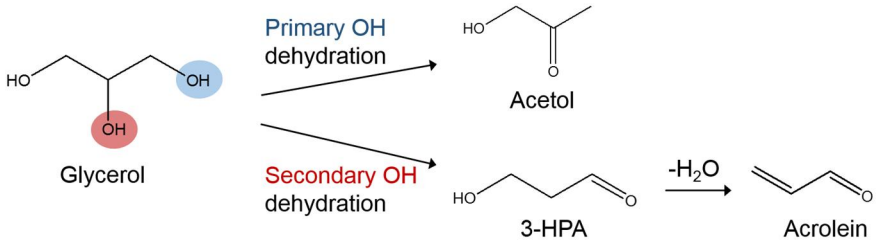

Scheme 2-1. Schematic diagram of glycerol dehydration

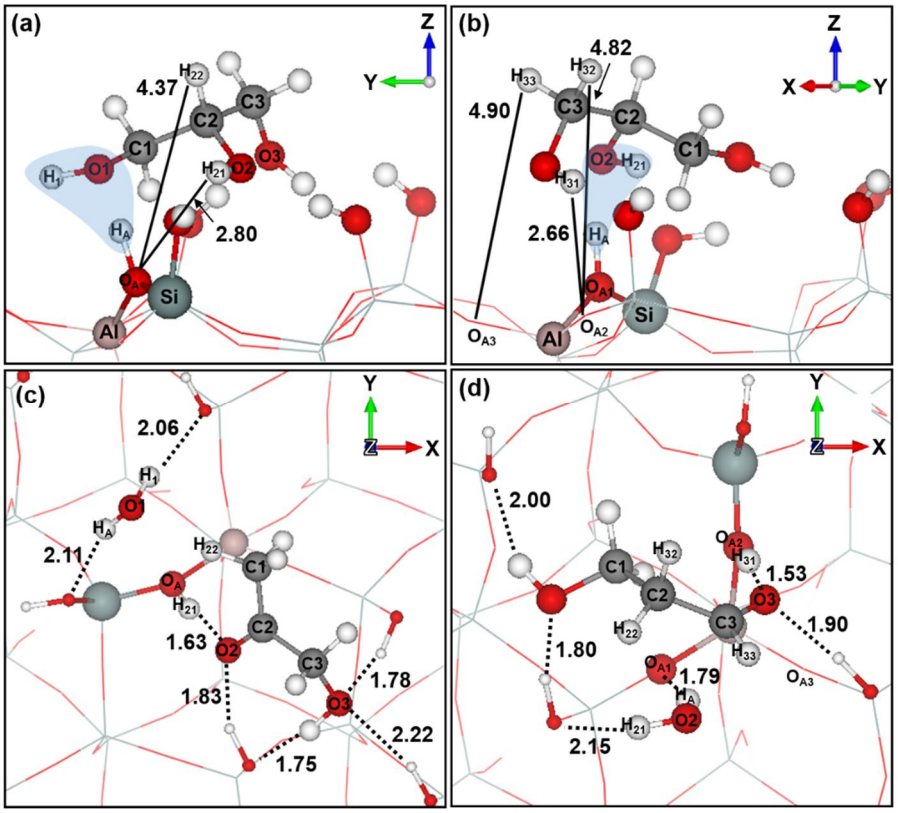

Figure 2-4. Optimized structures of (a) ads_primary, (b) ads_secondary, (c) ads_acetol+H_2O, and (d) ads_3-HPA+H_2O. The pink, light grey, gray, red, and white spheres (or lines) are for aluminum, silicon, carbon, oxygen, and hydrogen atoms, respectively. Blue highlighted remark: water formation / Dashed lines: hydrogen bonds

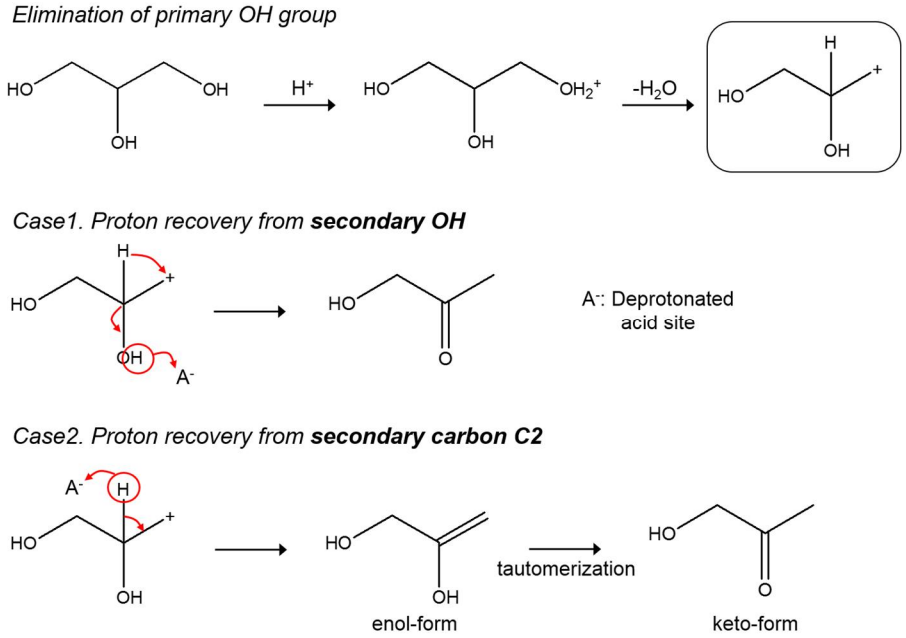

Scheme 2-2. Possible pathways depending on the recovery process of deprotonated acid site for acetol production from glycerol

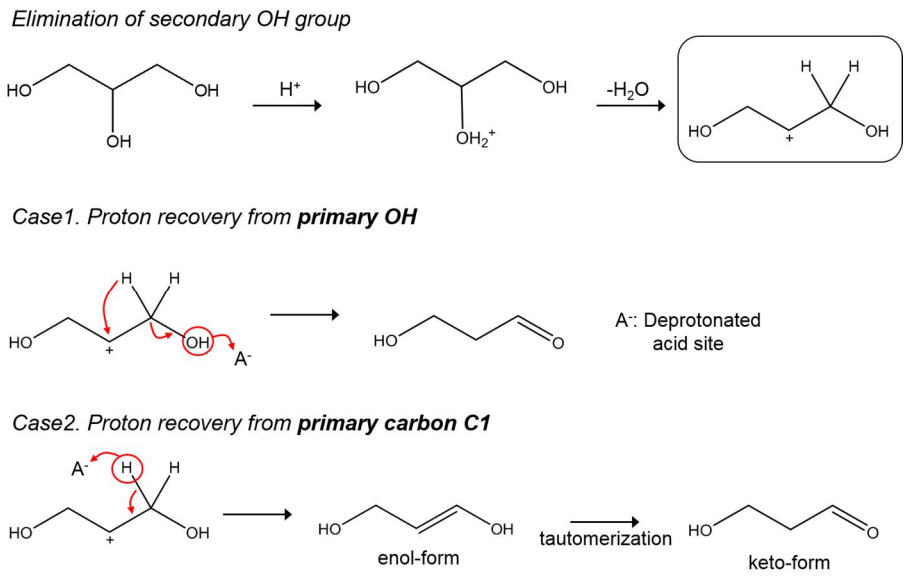

Scheme 2-3. Possible pathways depending on the recovery process of deprotonated acid site for 3-HPA production from glycerol

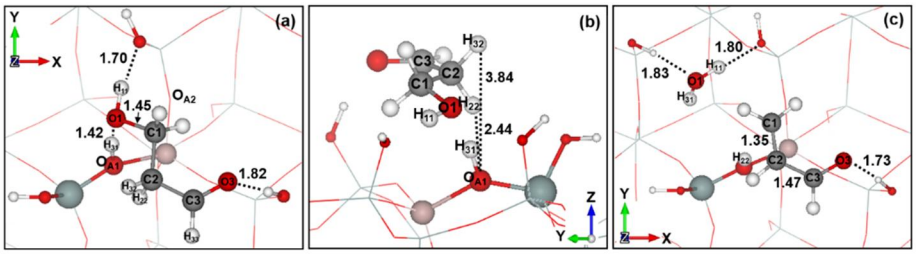

Figure 2-5. (a) Top and (b) side views of 3-HPA adsorption geometries, and (c) optimized structure of acrolein and water adsorption. The pink, light grey, gray, red, and white spheres (or lines) are for aluminum, silicon, carbon, oxygen, and hydrogen atoms, respectively.

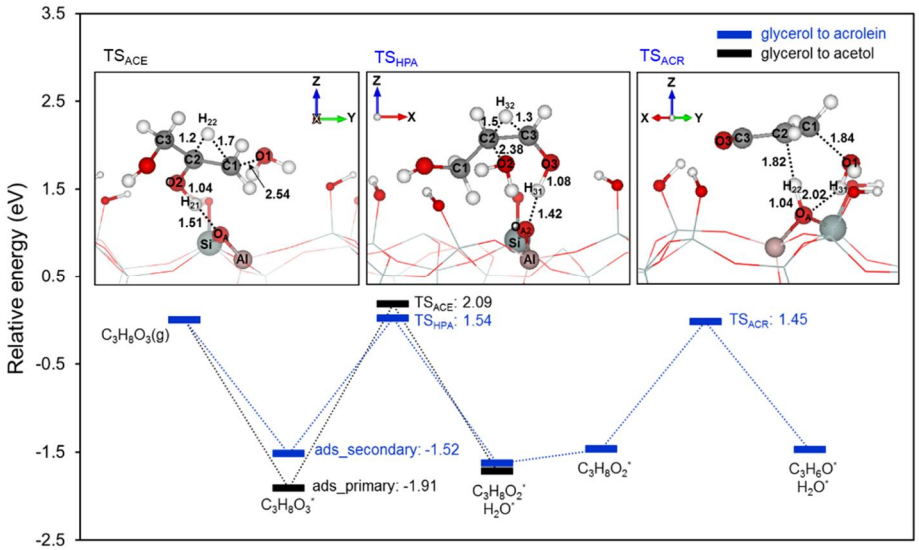

Figure 2-6. The energy profile of the glycerol dehydration on Si-(OH)-Al group of amorphous aluminosilicate. Energy is in eV relative to gas phase glycerol. Inset images: Optimized structures of transition state of each dehydration. The pink, light grey, gray, red, and white spheres (or lines) are for aluminum, silicon, carbon, oxygen, and hydrogen atoms, respectively.

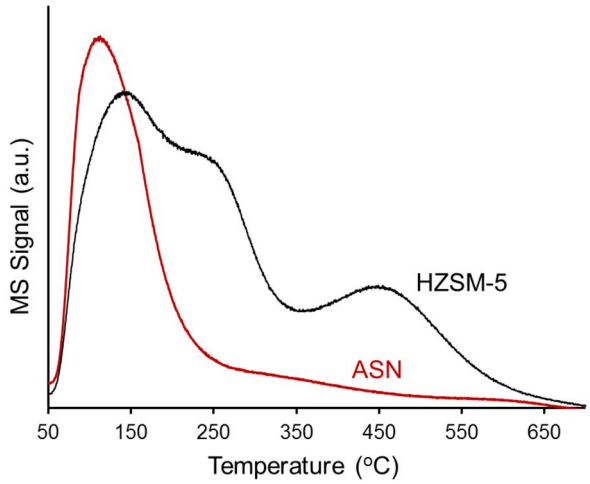

Figure 2-7. NH_3-TPD-MS profiles of HZSM-5 and ASN catalysts

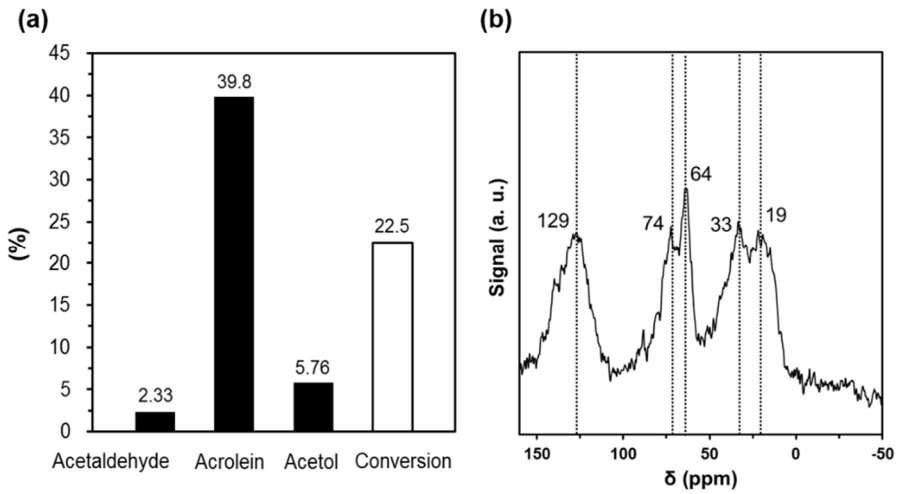

Figure 2-8. (a) Product distribution over ASN catalyst in glycerol dehydration at 1h (■: Selectivity for each product and □: Conversion) and (b) ^{13}C CPMAS NMR spectrum of used ASN catalyst

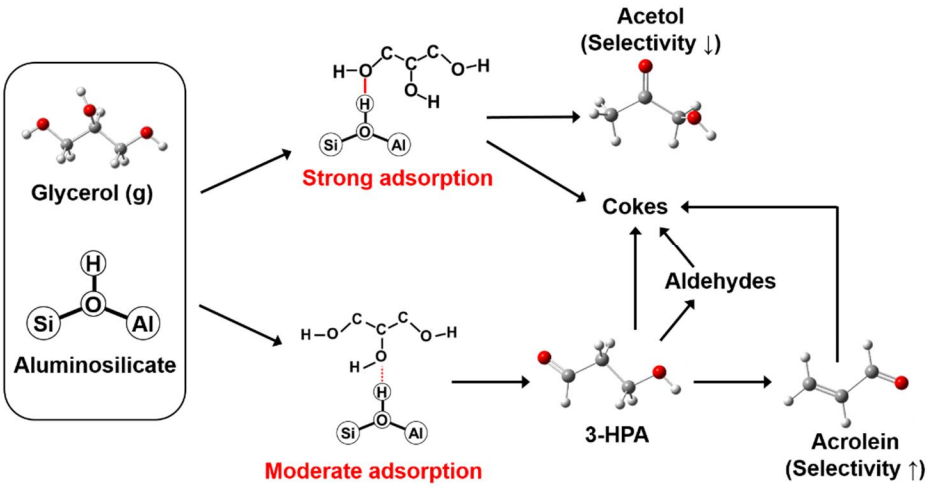

Scheme 2-4. Proposed mechanism for glycerol dehydration on Si-(OH)-Al group of amorphous aluminosilicate

Chapter 3. A tailored catalyst for the sustainable conversion of glycerol to acrolein: mechanistic aspect of sequential dehydration

3.1 Introduction

Thanks to previous studies, a better understanding has been developed regarding the mechanism of glycerol conversion [9, 11, 83] and the effectiveness of Brønsted acid catalysts [8, 13, 84, 85]. During glycerol conversion, a variety of reactions can take place, but the desired reaction are two sequential dehydrations consisting of the dehydration of glycerol to 3-hydroxypropionaldehyde (3-HPA) and 3-HPA to acrolein. When Brønsted acid catalysts are used, the first dehydration, known as the rate-determining step [64, 84], can be easily induced. This can be attributed to the secondary OH group of glycerol being preferentially adsorbed onto the Brønsted acid sites, which should occur prior to the dehydration to 3-HPA [8, 84]. Although Brønsted acid catalysts show a high activity and selectivity for acrolein early in the reaction, the catalysts are quickly deactivated due to extensive coke deposition [69, 70]. Therefore, solving the problem of coke formation is necessary to achieve glycerol dehydration on a commercial scale.

There are two approaches to solve the problem of this type of deactivation.

One involves reducing the amount of coke produced during the reaction and the other is enhancing intrinsic resistivity to coke deposition. For the former, a key to the solution involves 3-HPA conversion. 3-HPA is considered to be a major intermediate formed during the reaction as it is a precursor of acrolein [11, 67]. It is very reactive, and the additional undesired conversions can easily take place, resulting in coke formation.[9, 11, 67] However, the behavior of 3-HPA during glycerol dehydration is not well understood currently because the detection of 3-HPA is almost impossible during the reaction due to the highly reactive nature of 3-HPA. A theoretical study could contribute to a better understanding of this problem, but up to now such studies have been limited to the reaction mechanism of glycerol [83, 84]. It should be possible to observe the behavior of 3-HPA during the reaction using density functional theory (DFT) calculations.

The amount of coke produced can be reduced through the realization of appropriate active sites, but coke formation cannot be entirely prohibited considering the overall reaction. Therefore, enhancing the intrinsic resistivity of a catalyst to coke formation is essential for achieving a stable production of acrolein. In this regard, several attempts to control the textural properties of catalysts have been reported to improve coke resistivity. Tsukuda et al. [66] studied the influence of mesopore size of the silica support on catalytic stability. They demonstrated that the silica with the largest pores had the best resistance, thereby emphasizing the importance of pore size in the stable production of acrolein. On the other hand, Hoang et al. [86] examined suitable pore structures in terms of residence time of reactant or intermediate.

They found that compounds containing alkyl and aromatic groups were primarily formed over a catalyst with a longer residence time, which resulted not only in a low selectivity for acrolein but also in a rapid deactivation of the catalyst by coke deposition. Although enhancing effects caused by large pores and suitable pore structure were deduced, the problem associated with deactivation was not solved.

Herein, we propose the use of an open-macroporestructured and Brønsted-acidic silica (Marigold-like silica functionalized with propanesulfonic acid groups, MS-FS) as a sustainable and selective catalyst for acrolein production. The appropriate Brønsted acid sites for the sequential dehydration of glycerol were obtained through functionalization with propanesulfonic acid groups. In the dehydration of glycerol, the open-macropore structure of the catalyst showed a clear enhancement in resistance to hard coke formation and to pore blocking by coke. Using DFT calculations, we found a relationship between the behavior of 3-HPA and the recyclability of Brønsted acid sites during sequential dehydration. The MS-FS catalyst permitted the deprotonated Brønsted acid sites to be easily regenerated, which led to the selective dehydration of 3-HPA into acrolein. Moreover, the formation of coke precursors originating from the degradation of 3-HPA was inhibited. For these reasons, the MS-FS catalyst showed outstanding selectivity for acrolein formation and was also quite stable (with yields approaching 73% after 50 h).

3.2 Experimental

3.2.1 Preparation of catalysts

MS-FS was synthesized by a water-in-oil microemulsion process using a hydrothermal reactor. A synthetic method for marigold-like silica (MS) was published by Park et al. [87]. Urea (0.6 g) and cetylpyridinium bromide (1.0 g) were dissolved in water (30 mL). Tetraethyl orthosilicate (2.5 g), pentanol (1.5 mL), and cyclohexane (30 mL) were mixed. The two solutions were mixed for 30 min, and the mixture was prehydrolyzed at 120 ^{o}C for 2.5 h in an autoclave while stirring. After the reaction, the sample was cooled to room temperature and 3-mercaptopropyl trimethoxy silane (0.62 g) was slowly added while stirring. The sample was prepared in the same way as for prehydrolyzation, with the only difference being a 4 h reaction time. The product was centrifuged three times using a mixture of deionized water (15 mL) and acetone (15 mL). After that, the resulting material was dried at room temperature and grinded to a fine powder. To remove the surfactant, ethanol extraction was conducted because the functional groups can be oxidized through heat treatment or calcination. The sample (1 g) was suspended in ethanol (250 mL). After stirring at 75 ^{o}C for 24 h, a precipitate was obtained by centrifugation and dried at room temperature. Then, the sample (1 g) was oxidized using hydrogen peroxide (80 g; 34.5 wt%) at 60 ^{o}C for 24 h followed by washing with deionized water and ethanol. Finally, the product was dried at 70 ^{o}C for 12 h. Zirconia supported on silica (7 wt%)

was synthesized using an incipient wetness impregnation method. Zirconium oxychloride was dissolved in deionized water, and the marigold-like silica was impregnated with the solution. The sample was then dried at 80 ^{o}C overnight and calcined at 300 ^{o}C for 2 h. The calcined sample (0.5 g) was treated with sulfuric acid (10 mL; 0.5m, 95%) at room temperature for 30 min and calcined again at 650 ^{o}C for 3 h.

3.2.2 Catalyst characterization

To record the morphology of the samples, we carried out electron microscopy. HR-TEM and SEM images were obtained using a JEOL JEM-3010 and SUPRA 55VP microscope, respectively. An analytical high-angle annular dark-field scanning transmission electron microscope (HAADF-STEM, Tenai F20-FEI, 200 kV) equipped with EDS (Tecnai 136-5-EDAX) was used for elemental mapping of the sample. Nitrogen adsorption–desorption isotherms were recorded on a Micrometrics ASAP-2010, and the pore size distribution was determined from the branches of the isotherm using the Barrett–Joyner–Halenda method. Elemental analysis (CHNS0932, LECO) was conducted to determine the amount of sulfur in samples before and after the reaction. XRD patterns were obtained at angles ranging from 10–80 ^{o} using a Rigaku D-MAX2500-PC powder X-ray diffractometer with CuKa radiation (1.5406 Å). The chemical structure of the catalyst was confirmed using a FTIR spectrophotometer (Nicolet 6700, Thermo Scientific). TPO and NH_3-TPD results were obtained using a Micromeritics

Autochem II chemisorption analyser with an on-line mass spectrometer (QGA, HIDEN ANALYTICAL).

In the case of TPO analysis, the sample was loaded onto the reactor and heated up to 100 ^{o}C under a helium flow to vaporize the physically adsorbed molecules. After waiting for 1 h, the temperature was cooled to 50 ^{o}C. The data was collected while the temperature was increased to 600 ^{o}C at a rate of 5 ^{o}C·min^{-1} under a flow of 10% O_2/He. In the case of NH_3-TPD analysis, the sample was pretreated with 10.2% NH_3/He gas at 50 ^{o}C. The temperature was increased to 100 ^{o}C under a He flow to eliminate physisorbed NH_3. After removing physisorbed NH_3, the temperature was cooled to 50 ^{o}C and increased again to 600 ^{o}C (10 ^{o}C·min^{-1}) under a flow of helium. The data was collected simultaneously.

3.2.3 Catalyst activity test

The catalytic activity test was conducted at 250 ^{o}C in a fixed-bed quartz reactor. Before the reaction, the catalyst was pretreated at 250 ^{o}C for 30 min under a flow of N_2 (30 mL·min^{-1}). For the longterm stability test of MS-FS, the catalyst (0.45 g) was loaded and a glycerol solution (1.2 M) was fed into the reactor using a syringe pump at a rate of 1.5 mL·h^{-1} under a flow of nitrogen (30 mL·min^{-1}). For the comparison test, the catalyst (0.3 g) was

loaded and a glycerol solution (1.2 M) was fed into the reactor using a syringe pump at a rate of 2.0 $mL \cdot h^{-1}$ to exactly observe the difference in catalytic activities. When the glycerol solution was injected, the temperature of the inlet line was heated to 270 ^{o}C to vaporize the reactant. After the gas-phase glycerol reacted, the products were condensed in a cold trap and analyzed using a gas chromatograph (Younlin ACME 6100) equipped with a flame ionization detector (FID) and an HP-Innowax capillary column.

3.2.4 Computational details

Plane-wave DFT calculations were performed using the Vienna Ab initio Simulation Package (VASP) code [35] implementing the generalized gradient approximation (GGA) of Perdew-Burke-Ernzerhof (PBE) exchange-correlation functional [36]. As an all-electron description, the projector augmented wave method (PAW) was used [37]. The energy cut-off for the plane-wave basis set expansion was set to 400 eV and the Brillouin zone was sampled using a 3 × 3 × 1 Monkhost–Pack k-point mesh. All structures were optimized until forces on all atoms were converged to <0.03 $eV \cdot Å^{-1}$. The electronic optimization steps were converged to $<2 \times 10^{-4}$ eV.

The model surfaces of propanesulfonic acid functionalized silica (MS-FS) and SZ/MS were constructed based on the model of Rozanska et al. [38] The (111) surface of β-cristobalite was used as the model to represent amorphous silica surface [40–42]. Physical properties, such as refractive index and bulk

density, of β-cristobalite fairly resemble those of amorphous silica [88, 89]. The most preferred structure was found through careful examination of possible structures, for example, location of propanesulfonic acid group and zirconium ion on the silica surface, and rotating angle between the surface and propanesulfonic acid group. In our calculations, all atomic positions were fully relaxed to move, and a sufficient distance between the two adjacent slabs was provided to avoid periodic interactions.

The climbing image-nudged elastic band (CI-NEB) method [45, 46] was used to determine transition states and energy barriers for the proton-exchange ability of the catalysts. A 1 × 1 × 1 Monkhost–Pack k-point mesh and a cut-off energy of 400 eV were used for these calculations. Initial reaction trajectories consisted of three images obtained through linear interpolation. To determine minimum energy paths, these images were optimized until the forces between the images fell to <0.06 eV·Å^{-1}.

3.3 Results and discussion

We designed and synthesized MS-FS (Scheme 3-1). The marigold-like structure accommodates the large openpore space between the silica walls and can enhance the mass transport of both the reactant and product. The unctionalization of the surface with propanesulfonic acid groups confers pure Brønsted-acidic characteristics to the catalyst. The importance of Brønsted acid type has been emphasized in previous reports [8, 13, 84, 85]. In the case of acidity, a narrow distribution of acid strength should be advantageous for the selective formation of the product. In this regard, the propane-sulfonic acid moiety can ensure uniformity of acid strength because the propyl chain in the moiety separates the acid site from the surface of the catalyst. The variability of acid site strength induced from the surface structure [90, 91] can be diminished, resulting in acid sites with identical strengths. We confirmed this effect of propanesulfonic acid group by performing simple cluster-based DFT calculations (Table 3-1). The deprotonation energy (ΔE_{DPE}, related to the strength of acid sites) of propanesulfonic acid group was essentially unaltered (≈24 $kJ \cdot mol^{-1}$) by the modification with a moiety attached to the terminal carbon atom. In contrast, a similar modification with sulfuric acid resulted in a significant change in ΔE_{DPE} (≈104 $kJ \cdot mol^{-1}$).

Figure 3-1 shows electron microscope images of the MS-FS catalyst. It can be clearly seen that MS-FS is a nanosphere with a size ranging from 400–600 nm. The surface of MS-FS is covered by winding walls of silica, and

deep canyons are formed between the walls (Figure 3-1(a) and (c)). In SEM images, the estimated distance between the silica walls ranges from 10 nm to over 100 nm. The thickness of each wall is estimated to be 13.1–17.5 nm based on Figure 3-1(a), but it can be thinner because of the platinum coating required for SEM analysis. In Figure 3-1(b), the wall thickness at the edge is about 3–5 nm. In the same image, pores formed between the silica walls are clearly observed. These pores appear to be formed from the inside to the outside of the nanospheres. In addition, very small white dots and fringes can be seen over the entire nanosphere. They are 2–5 nm-sized mesopores distributed in the silica walls and the inside of hierarchical structured pores, which was further confirmed by nitrogen physisorption analysis. Interestingly, although the propanesulfonic acid moieties were used to functionalize the catalyst, the overall catalyst structure was almost the same as that for a nonfunctionalized silica nanosphere, Marigold-like silica (MS).

Details concerning the pore structure and textural properties of the MS-FS catalyst were confirmed by nitrogen physisorption analysis. In the nitrogen isotherm plot (Figure 3-2(a)) of the MS and MS-FS catalysts, the broad hysteresis loop from 0.4 to 1.0 (P/P^0) indicates that meso- and macrosizded pores are present in the catalysts. A significant increase in adsorbed nitrogen in the range of 0.7 to 1.0 clearly shows that there is a considerable amount of macropores in both catalysts. The most notable difference between the MS and MS-FS catalysts is the amount of adsorbed nitrogen near P/P^0=0.4. In the case of nonfunctionalized MS, a sharp increase in adsorbed nitrogen was observed, which implies the presence of large amounts of mesopores. In

contrast, functionalized MS-FS does not show this sharp increase. The pore size distribution clearly shows this difference between the absence and presence of

functional groups (Figure 3-2(b)). The amount of 2–5 nm-sized mesopores was definitely decreased as a result of functionalization. This can be attributed to the length of the propanesulfonic acid moiety (0.68–0.75 nm), which is sufficiently long to block small pores. In addition, this distinct difference in the amount of mesopores indicates that small mesopores are regularly distributed not only on the inside of hierarchically structured pores but also in the silica walls. This result is in good agreement with the observation of white dots and fringes in the TEM image (Figure 3-1(b)). The amount of macropores decreased because the thickening of the walls made the distance between the walls shorter. From these results, we confirmed that functionalization was successfully carried out and that hierarchically structured meso–macropores were well developed in the MS-FS catalyst.

Successful functionalization of MS-FS was also confirmed by elemental analysis. In MS-FS, the weight percentage of sulfur was estimated to be 1.4 %. In addition, the structure of the functional groups was confirmed by FTIR analysis.

The activity of the MS-FS catalyst was investigated for glycerol dehydration. Although the reaction was run for 50 h, the glycerol conversion was maintained at 100% and the selectivity for acrolein was high (72.8 %; Figure 3-3). Considering previous studies, which attempted to solve the deactivation problem by co-feeding oxygen [92] or adding a promoter, [93–

95] the selectivity for acrolein and the stability of MS-FS are outstanding. To further investigate the reason why MS-FS showed such a high stability, we carried out comparative studies with regard to i) hierarchically structured meso–macropores and ii) characteristics of Brønsted acid sites.

Extensive coke formation on the acid sites is a typical problem in glycerol dehydration.[69, 70] Coke deposition could lead to the blockage of pore entrances, resulting in rapid deactivation. Therefore, proper textural properties such as a large pore size and hierarchical pore structures are the major factors in terms of catalyst stability. For this reason, we selected zeolite HZSM-5 as a control group with microporous structures and compared the catalytic activities of both catalysts. Fresh HZSM-5 has a crystal structure, as evidenced by high-resolution HR-TEM and XRD analysis. Nitrogen adsorption–desorption isotherms showed no distinct hysteresis loop (Figure 3-4(c)), which indicates that the fresh HZSM-5 catalyst has a typical microporous structure unlike the MS-FS catalyst.

As shown in Table 3-2, HZSM-5 was initially active and selective for the production of acrolein (conversion 92.7 % and selectivity 73.0 %), similar to previous results [69]. However, the catalyst was rapidly deactivated even though its selectivity was maintained. The conversion of glycerol after a 10 h reaction was only 21.9 %. The major by-product, acetol, formed with the same selectivity (9.3 %) using MS-FS, and other by-products formed at yields of nearly 0 % for both catalysts.

The used catalysts were analyzed by using the nitrogen adsorption method, and a dramatic change in porosity was found. Figure 3-4(a) and (b) shows

the pore size distribution of HZSM-5 and MS-FS, respectively. In the case of HZSM-5, after 10 h reaction, the micro-sized pores were completely blocked due to coke deposition. In contrast, macropores of 20–100 nm in MS-FS were still present even after 30 h reaction. The difference between HZSM-5 and MS-FS is also presented in the isotherms of fresh and used samples (Figure 3-4(c) and (d)). The amount of adsorbed nitrogen for used HZSM-5 was significantly decreased in the range below 0.2 (P/P^0 ; region related to micropores), and the isotherm was down-shifted. On the other hand, most of the nitrogen adsorption (P/P^0 >0.6) for the used MS-FS was still maintained. The results explain why the MS-FS catalyst showed a remarkable stability in spite of extensive coke formation. The hierarchically structured meso–macropores in MS-FS confer an advantage in that pore blocking is reduced, resulting that acid sites located inside the pores can remain functioning for a long reaction time.

In addition, the properties of the coke on the two catalysts were different from each other. Figure 3-5 shows the temperature-programmed oxidation (TPO) results for the used catalysts. The oxidation of coke in MS-FS starts at 220 ^{o}C, which is a lower temperature compared with that for HZSM-5, 270 ^{o}C. In addition, the major oxidation peak appears at 330 ^{o}C in the MS-FS catalyst whereas that of HZSM-5 appears at 509 ^{o}C. This is because the coke in HZSM-5 is likely to be polymerized or condensed due to the microporous structure of the catalyst. Also, by comparing the integrated area of TPO profiles in both catalysts, it can be seen that the amount of coke produced is similar. As frequently pointed out, the stability of MS-FS is superior to

HZSM-5 although a similar amount of coke was deposited during the reaction. These results can be explained by a study reported by Hoang et al. [86]. In the meso–macropores of MS-FS, the residence time of intermediates or coke precursors can be reduced, which results in a decrease in the probability of coke polymerization.

A comparison of the Brønsted acid sites was carried out using sulfated zirconia supported on the marigold-like silica (SZ/MS) and MS-FS catalysts. The morphology of the SZ/MS catalyst was confirmed to be identical with that of MS-FS (Figure 3-6(a)–(d)); the use of the same morphology can diminish the effect of pore structure. As shown in the 2D nergy dispersive X-ray spectroscopy (EDS) mapping images of SZ/MS (Figure 3-6(e)–(h)), sulfated zirconia was highly dispersed on the MS support. Only a broad amorphous silica peak corresponding to SZ/MS is observed, which is also consistent with the sulfated zirconia being highly dispersed in the SZ/MS catalyst. The loaded amount of sulfur was estimated by elemental analysis. The weight percentage of sulfur in the SZ/MS is same as that in the MS-FS catalyst. This indicates that the amount of functional groups is identical in both fresh MS-FS and SZ/MS catalysts.

The acid sites of the sulfated zirconia exhibit Brønsted-acidic characteristics that are structurally similar to the sulfonic acid moiety of MS-FS [96]. The major differences in acid sites between SZ/MS and MS-FS are acid strength and uniformity of acid site distribution. Temperature-programmed desorption of NH_3 (NH_3-TPD) results for MS-FS and SZ/MS are presented in Figure 3-7. NH_3 desorption in the case of MS-FS started at

100 °C and ended at around 300 °C. In the case of SZ/MS, the desorbed NH_3 was detected in the broad temperature range from 120–480 °C. The higher temperature of NH_3 desorption in the case of SZ/MS suggests that the SZ/MS catalyst exhibit a slightly stronger acidity than the MS-FS catalyst. Moreover, MS-FS showed a narrower NH_3 desorption peak than SZ/MS, which indicates that acid sites in MS-FS are uniformly distributed. This result is consistent with cluster-based DFT calculation results. Considering the uniform distribution of the acid sites, the selectivity for acrolein of MS-FS was expected to be superior to that of SZ/MS.

Experimental results show that the SZ/MS catalyst has a low glycerol conversion and selectivity for acrolein, which is a completely different to the result for the MS-FS catalyst (Table 3-3). The deactivation behavior in SZ/MS was also distinct from that of MS-FS. Even though both catalysts have almost identical textural properties, glycerol conversion using SZ/MS decreased with increasing time on stream (TOS). After the reactions, we analyzed the amount of sulfur in both used catalysts because sulfonic acid groups or sulfuric acid groups can be detached from the silica support. The weight percentage of sulfur remained unchanged in both catalysts. This indicates that the main reason for the deactivation of SZ/MS is not the leaching of sulfur from the catalyst or pore blocking.

The low selectivity for acrolein is explained by the fact that SZ/MS has a stronger acid strength than MS-FS. Too strong Brønsted acid sites could result in a significant formation of by-products because many side reactions are also catalyzed by Brønsted acid sites during glycerol dehydration [83].

However, the formation of a considerable amount of acetaldehyde (8.6% in SZ/MS.) cannot be solely explained by the difference in acid strength. It was reported that the formation of acetaldehyde stems from the homogeneous decomposition of 3-HPA [9, 67, 97]. Therefore, the formed 3-HPA was preferentially desorbed from the acid sites of the SZ/MS catalyst and then homogeneous decomposition to acetaldehyde occurred. To explain such a difference, we anticipated that the 'reversibility' of the Brønsted acid site was the reason for the difference between the MS-FS and SZ/MS catalysts. Herein, the term reversibility is similar to the ability of recovering protons from reaction intermediates.

Scheme 3-2 shows a proposed reaction mechanism accounting for the reversibility of each catalyst. In both catalysts, glycerol is converted into 3-HPA through protonation and dehydration. After this, in the case of the easily reversible MS-FS catalyst, a proton is readily transferred to an acid site to regenerate the Brønsted acidity. Over regenerated sites, 3-HPA is readily adsorbed on an acid site by hydrogen bonding and selectively dehydrated to acrolein. In contrast, the reversibility of SZ/MS is somewhat lower than that of MS-FS, and the recovery of a proton for SZ/MS is more difficult than for MS-FS. When the deprotonated sites are readily regenerated in SZ/MS, the reaction of 3-HPA would follow the same route as that on the MS-FS catalyst. On the other hand, when deprotonated sites are not regenerated, 3-HPA can be desorbed from the active site due to the absence of interactions and would decompose into formaldehyde and acetaldehyde. These compounds can participate in side reactions to form

coke [9, 11, 67]. Therefore, we expect that this difference is the reason why the SZ/MS catalyst exhibits different catalytic activities compared to the MSFS catalyst.

To verify the proposed scheme, we compared the recyclability of acidic protons for each catalyst using DFT calculations. In the elementary steps of a typical dehydration [10], the reaction is initiated by the migration of a proton from a Brønsted acid site to the reactant. Then, the protonated reactant undergoes dehydration and a charged intermediate is formed. Finally, the proton is pulled out from the charged intermediate with the Brønsted acidity being recovered. As already noted, we anticipate that the last step is probably important in the sequential dehydration of glycerol.

In the calculation, a water molecule was used as a probe to investigate the recyclability of the MS-FS and SZ/MS catalysts. Figure 3-8 shows the optimized structures for the overall dehydration process, which consists of the adsorption of water, proton transfer from a Brønsted acid site to water, and the recovery of a proton from a hydronium ion. To describe proton transfer and recovery, we simulated a water-assisted proton exchange. The adsorption energies of water on the MS-FS and SZ/MS surfaces were -39.8 and -49.6 $kJ \cdot mol^{-1}$, respectively. The activation energy required for the transfer of a proton from MS-FS was 111.4 $kJ \cdot mol^{-1}$, which was higher than that for SZ/MS (79.2 $kJ \cdot mol^{-1}$, Figure 3-9). This result is consistent with experimental observations (NH_3-TPD–MS, Figure 3-7) because the lower

protonation energy corresponds to a catalyst with a stronger acidity. At the same time, however, the recovery of a proton from a hydronium ion over the MS-FS catalyst is more thermodynamically favored than the analogous process for SZ/MS due to the higher stabilization energy of proton extraction (-111.4 vs. -79.2 $kJ \cdot mol^{-1}$). Therefore, the recyclability of SZ/MS was inferior to that of MS-FS, which resulted in the generation of deprotonated acid sites. Over the deprotonated acid sites, the adsorption of 3-HPA was not favorable as the calculated energy was only -1.9 $kJ \cdot mol^{-1}$, which was negligible compared to -56.2 $kJ \cdot mol^{-1}$ for the initial acid site. In this situation, 3-HPA can be readily desorbed from the site and decomposition to acetaldehyde and formaldehyde would be expected to follow. Based on these computational calculations, we confirmed that the proposed reaction mechanism in MS-FS and SZ/MS catalysts is reasonable. In addition, it cannot be emphasized enough that not only appropriate acidity but also the recyclability of acid sites is a crucial factor for the selective and stable production of acrolein in the sequential dehydration of glycerol.

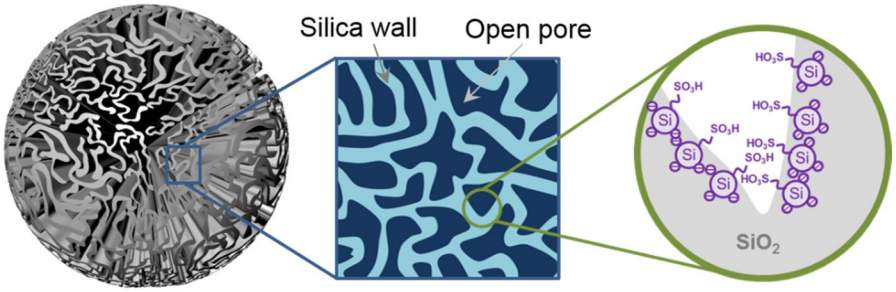

Scheme 3-1. Description of MS-FS catalyst on various scales.

Table 3-1. Effect of modification in terminal carbon on the de-protonation energy (ΔE_{DPE}) of propanesulfonic acid and sulphuric acid: Cluster based DFT calculations

Model	Structure	Terminal group	ΔE_{DPE}[a] (kJ/mol)	Variation[b] (kJ/mol)
$CH_3(CH_2)_2SO_3H$		-	475.9	-
CH_3 $(CH_2)_3SO_3H$	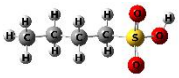	CH_3	475.8	0.1
SiH_3 $(CH_2)_3SO_3H$	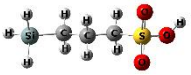	SiH_3	467.2	8.7
AlH_2 $(CH_2)_3SO_3H$		AlH_2	472.7	3.2
ZrH_3 $(CH_2)_3SO_3H$		ZrH_3	451.8	24.1
H_2SO_4		-	427.2	-
SiH_3 SO_4H		SiH_3	422.4	4.8
AlH_2 SO_4H		AlH_2	369.7	42.5
ZrH_3 SO_4H	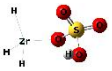	ZrH_3	323.3	103.9

[a] Respect to following reaction: $HA + NH_3 \rightarrow A^- + NH_4^+$ and

[b] Difference of ΔE_{DPE} compared to $CH_3(CH_2)_2SO_3H$ or H_2SO_4

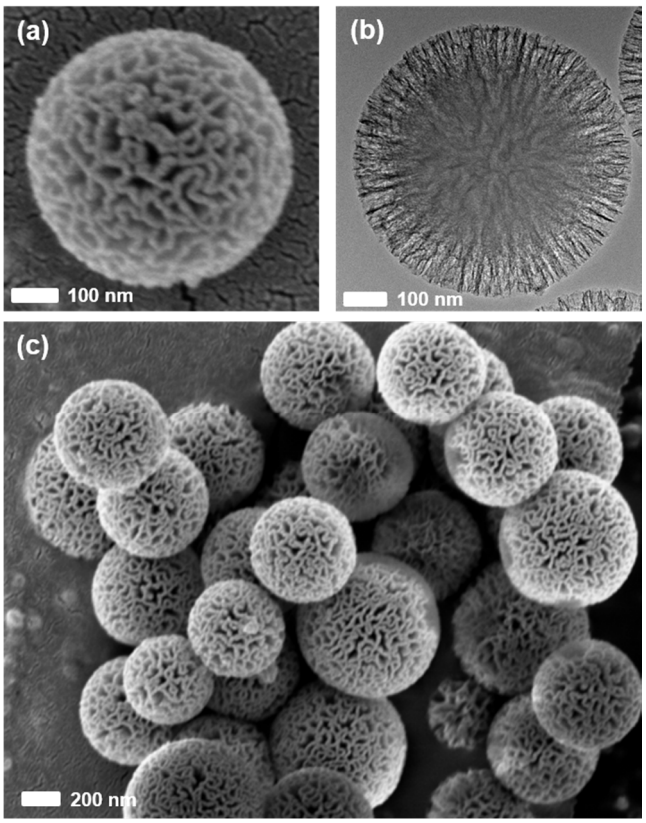

Figure 3-1. Electron microscope images of MS-FS catalyst: (a, c) SEM and (b) TEM.

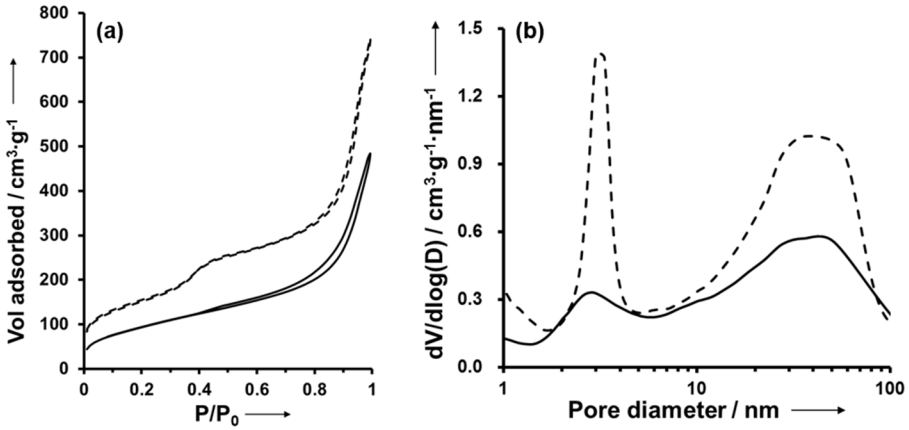

Figure 3-2. a) N_2 adsorption-desorption isotherm and (b) pore size distribution curve of MS-FS(──) and MS(----).

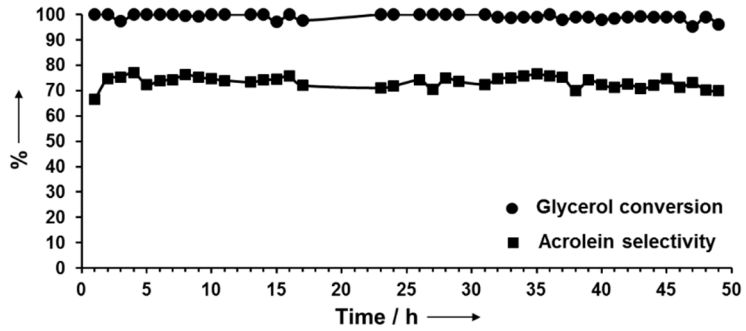

Figure 3-3. Glycerol conversion (●) and acrolein selectivity (■) of MS-FS.

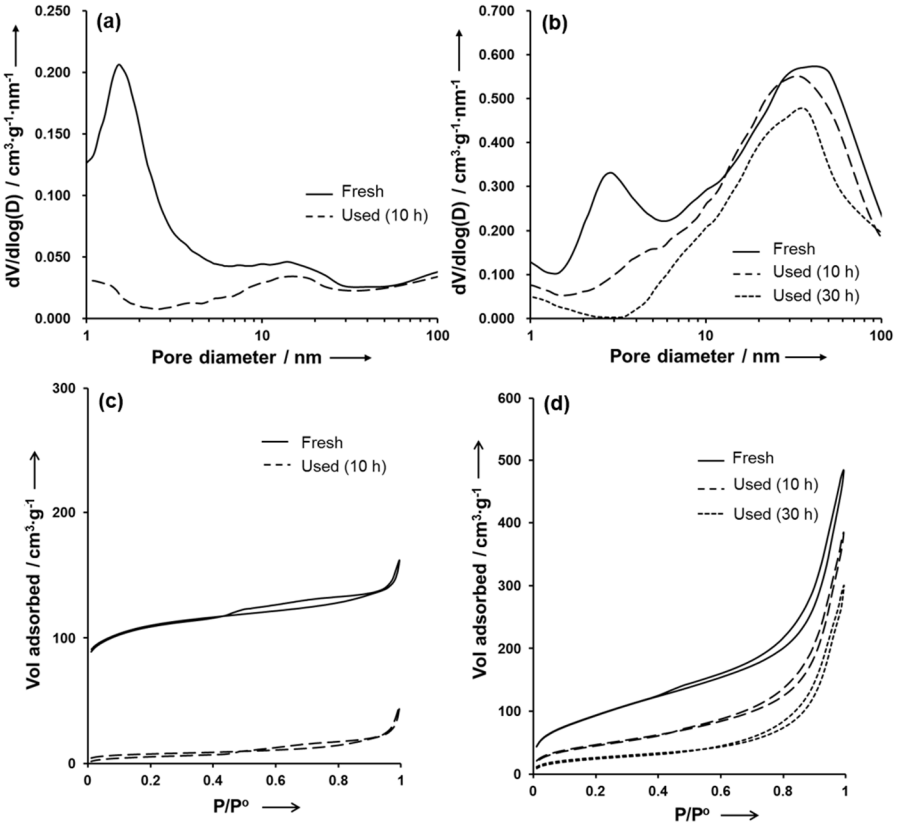

Figure 3-4. Pore size distribution of (a) HZSM-5 and (b) MS-FS catalysts for fresh samples and those used for 10 and 30 h. Nitrogen adsorption–desorption isotherms of (c) HZSM-5 and (d) MS-FS catalysts.

Table 3-2. Effect of modification in terminal carbon on the de-protonation energy (ΔE_{DPE}) of propanesulfonic acid and sulphuric acid: Cluster based DFT calculations

Catalyst	TOS=1-2 h	TOS=9-10 h	S_{ACR}[a] /%	S_{ACE}[b] /%	S_{AAL}[c] /%
	Glycerol Conversion/%	Glycerol Conversion/%			
HZSM-5	92.7	21.9	73.0	9.3	0.0
MS-FS	100.0	100.0	73.4	9.3	0.0

Selectivity for [a] acrolein, [b] acetol and [c] acetaldehyde

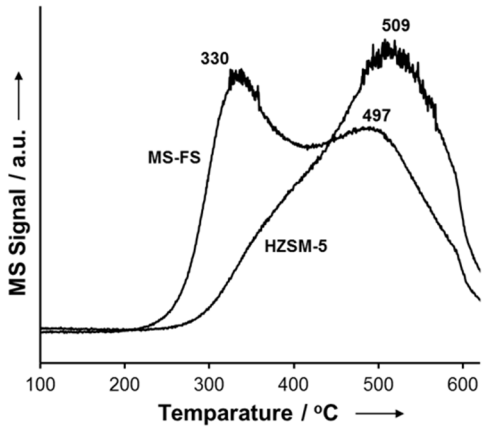

Figure 3-5. TPO-MS profiles of MS-FS and HZSM-5 after 10 h glycerol dehydration.

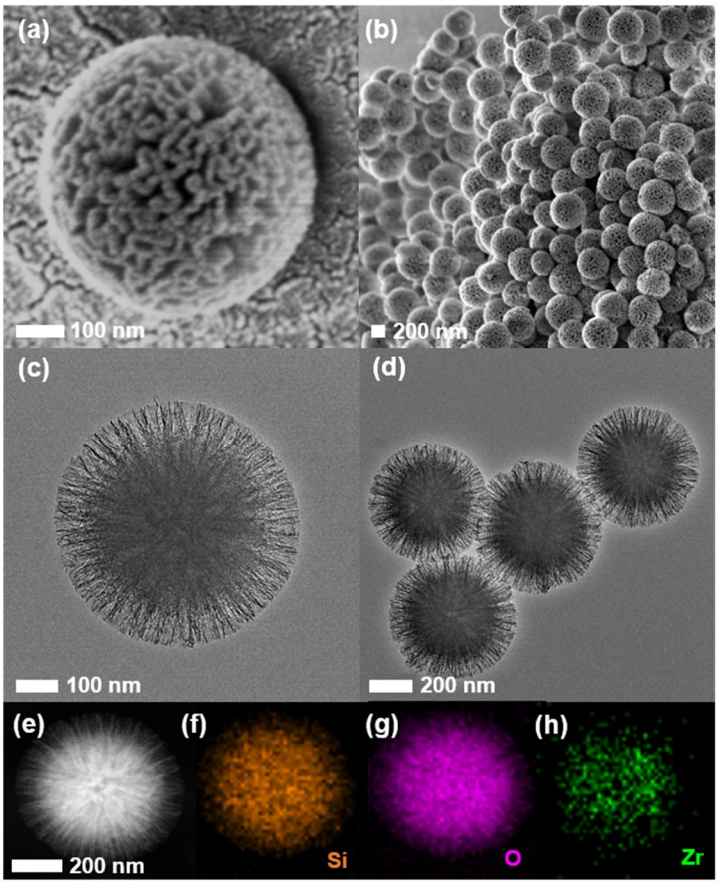

Figure 3-6. (a, b) SEM, (c, d) HR-TEM, (e) high-angle annular dark-field scanning transmission electron microscope (HAADF-STEM), and (f–h) EDS mapping images of the SZ/MS catalyst.

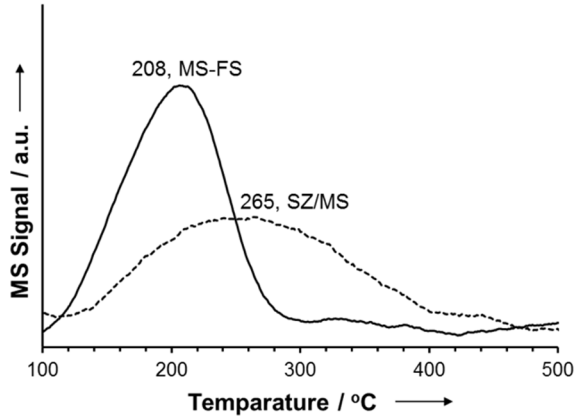

Figure 3-7. NH_3-TPD–MS profiles of MS-FS and SZ/MS.

Table 3-3. Catalytic activity of MS-FS and SZ/MS catalysts in the dehydration of glycerol as time on stream. The amount of catalyst: 0.3 g, glycerol feed rate: 2.0 ml/h and reaction temperature: 250 ^{o}C

Catalyst	TOS=1-2 h	TOS=9-10 h	S_{ACR}[a] /%	S_{ACE}[b] /%	S_{AAL}[c] /%
	Glycerol Conversion/%	Glycerol Conversion/%			
SZ/MS	76.8	56.8	18.3	10.7	8.6
MS-FS	100.0	100.0	73.4	9.3	0.0

Selectivity for [a] acrolein, [b] acetol and [c] acetaldehyde

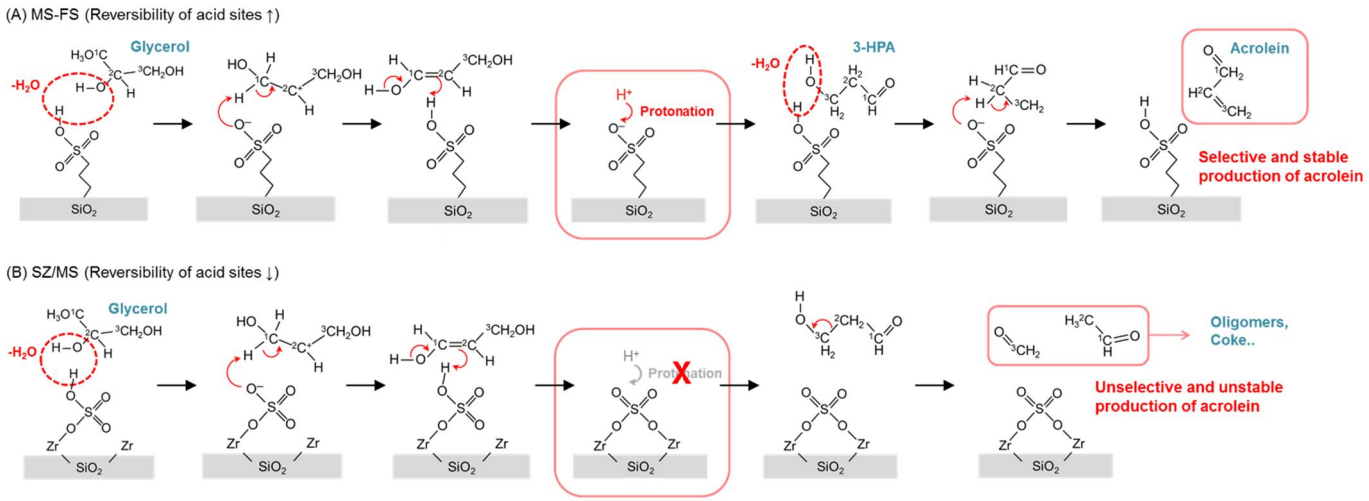

Scheme 3-2. Proposed mechanism concerning recyclability of a Brønsted acid site in (A) MS-FS and (B) SZ/MS catalysts.

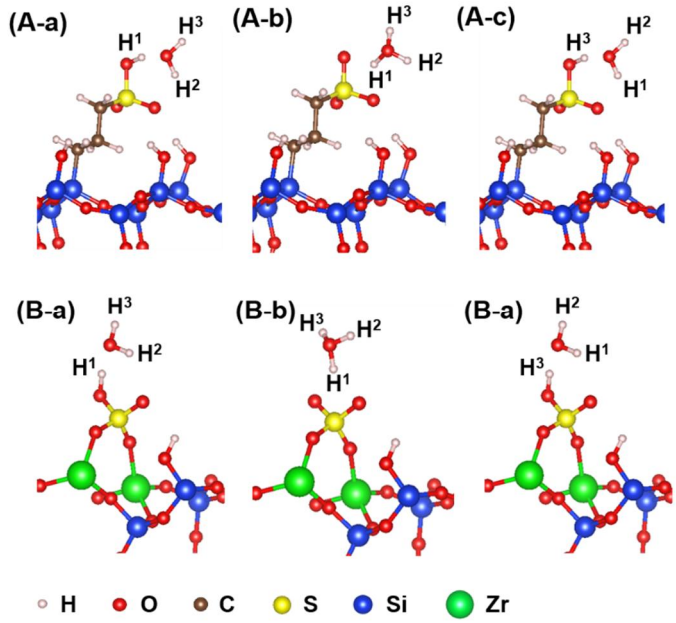

Figure 3-8. (a, c) Adsorption geometries and (b) transition state for water-assisted proton transfer reaction on (A) MS-FS and (B) SZ/MS catalysts.

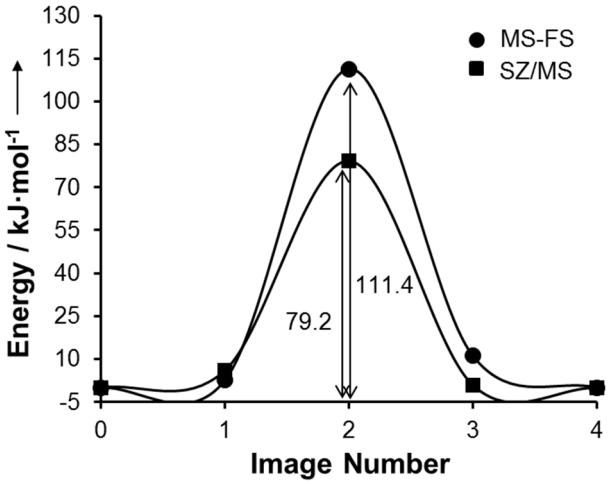

Figure 3-9. Density functional theory calculations of the minimum energy path for water-assisted proton exchange over MS-FS and SZ/MS surfaces.

Chapter 4. Summary and Conclusions

The design of a sustainable catalyst for glycerol dehydration based on mechanistic study were reported. In order to investigate the glycerol dehydration mechanism using DFT calculations, an amorphous aluminosilicate surface was constructed based on a β-cristobalite crystal which is a representative structure of amorphous silica. In the reaction networks, the adsorption and activation energies in each elementary step were calculated. The first dehydration step was identified as a rate-determining step in glycerol dehydration, which agreed well with a previous report. In the first dehydration, glycerol was converted into either 3-HPA or acetol, which was determined by the OH group of glycerol that was abstracted first in the ratedetermining step. When glycerol was adsorbed with the second OH group on the acid site, the adsorption energy was -1.52 eV. Compared to the ads_primary case (-1.91 eV), the adsorption strength of the glycerol of ads_secondary was relatively moderate. In addition, the activation energy for 3-HPA production was lower (1.54 eV) than that for acetol production (2.09 eV). These calculated results suggested that 3-HPA and water are favorably produced in the first dehydration on an amorphous aluminosilicate surface. The activation energy for 3-HPA dehydration was 1.45 eV, which demonstrated that 3-HPA is readily converted into acrolein and water by the second dehydration, and acrolein is the main product in the glycerol dehydration. The predicted selectivity for each product was verified via

catalytic activity test. Amorphous aluminosilicate showed outstanding selectivity for acrolein (39.8%) compared with its selectivity for acetol (5.76%), which agreed well with our theoretical prediction. In addition, adsorbed glycerol and its polymerized form were observed in the used catalyst. This reveals that glycerol that is too strongly adsorbed is difficult to convert, which facilitates coke deposition. The findings suggested that the silanol groups on aluminosilicate surface lead to different adsorption energy, reaction process, and coking from those of H-ZSM-5 zeolite in spite of the similar active sites, Si-(OH)-Al groups.

We designed and successfully synthesized a hierarchical-porestructured and propanesulfonic-acid-functionalized silica catalyst (MS-FS) to stably produce acrolein from glycerol. As expected, the MS-FS catalyst showed an outstanding selectivity (~73%) and stability (50 h) during the sequential dehydration of glycerol to acrolein. Compared to a microporous HZSM-5 zeolite, the hierarchically structured meso–macropores in MS-FS were strongly resistant to the blocking of pore entrances by coke deposition. Moreover, the formed coke was confirmed to be more easily oxidized than the highly condensed coke formed in the case of HZSM-5. As a consequence, acrolein was stably produced using the MS-FS catalyst, even after a considerable amount of coke had been deposited. In addition, we found that the recyclability of deprotonated Brønsted acid sites is a significant factor in the sequential dehydration of glycerol. If the recyclability of a catalyst is sufficient, the regeneration of deprotonated Brønsted acid site easily takes place. In this case, 3-HPA formed from the first dehydration of glycerol is

favorably adsorbed onto the regenerated Brønsted acid site followed by dehydration into acrolein in the subsequent step. However, in the case of a catalyst with a low recyclability, the regeneration of the deprotonated acid sites is retarded and the probability of 3-HPA being desorbed from the active site increases, resulting in a high likelihood of decomposition into acetaldehyde and formaldehyde. DFT calculations revealed that the MS-FS catalyst had an improved regeneration ability of deprotonated Brønsted acid sites compared to that of sulfated zirconia supported on silica (SZ/MS). Therefore, the sequential dehydration is easily achieved in the case of the MS-FS catalyst with a high selectivity for acrolein. Furthermore, catalyst stability is also enhanced because the formation of coke precursors generated from the degradation of 3-HPA is inhibited at the regenerated acid sites.

Bibliography

[1] B. Liu and Z. Zhang, *ACS Catal* **2016**, 6, 326-338.

[2] Y. Nakagawa, K. Tomishige, *Catal. Sci. Technol.* **2011**, 1, 179-190.

[3] B. Katryniok, S. Paul, F. Dumeignil, *ACS Catal.* **2013**, 3, 1819-1834.

[4] D. Suna, Y. Yamadaa, S. Satoa, W. Ueda, *Appl. Catal. B: Environ.* **2016**, 193, 75-92

[5] L. Liu, X.P. Ye, J.J. Bozell, *ChemSusChem* **2012**, 5, 1162-1180.

[6] A. Talebian-Kiakalaieh, N.A.S. Amin, H. Hezaveh, *Renew. Sustain. Energy Rev.* **2014**, 40, 28–59.

[7] Y. Choi, H. Park, Y.S. Yun, J. Yi, *ChemSusChem* **2015**, 8(6), 974-979.

[8] A. Alhanash, E.F. Kozhevnikova, I.V. Kozhevnikov, *Appl. Catal. A: Gen*. **2010**, 378, 11–18.

[9] A. Corma, G.W. Huber, L. Sauvanaud, P. O'Connor, *J. Catal.* **2008**, 257, 163-171.

[10] K. Kongpatpanich, T. Nanok, B. Boekfa, M. Probst, J. Limtrakul, *Phys. Chem. Chem. Phys.* **2011**, 13, 6462-6470.

[11] W. Suprun, M. Lutecki, T. Haber, H. Papp, *J. Mol. Catal. A: Chem.* **2009**, 309, 71-78.

[12] G. Busca, *Chem. Rev.* **2007**, 107, 5366–5410.

[13] Y. Choi, D.S. Park, H.J. Yun, J. Baek, D. Yun, J. Yi, *ChemSusChem* **2012**, 5(12), 2460–2468.

[14] W. Buhler, E. Dinjus J. *Supercrit. Fluids,* **2002**, 22, 37-53

[15] L. Ott, M. Bicker *Green Chem.* **2006**, 8, 214-220

[16] S. Ramayya, A. Brittain *Fuel* **1987**, 66, 1364-1371

[17] M. Aresta, A. Dibenedetto, *J. Braz. Chem. Soc.* **2014**, 25, 2215-2228.

[18] M. Trombetta, G. Busca, S. Rossini, V. Piccoli, U. Cornaro, A. Guercio, R. Catani, R.J. Willey, *J. Catal.* **1998**, 179, 581-596.

[19] B. Xu, C. Sievers, J.A. Lercher, J.A. Rob van Veen, P. Giltay, R. Prins, J.A. van Bokhoven, *J. Phys. Chem. C* **2007**, 111, 12075-12079.

[20] C. Chizallet, P. Raybaud, *Angew. Chem. Int. Ed.* **2009**, 48, 2891-2893.

[21] E.J.M. Hensen, D.G. Poduval, V. Degirmenci, D.A J. Michel Ligthart, W. Chen, F. Maugé, M.S. Rigutto, J.A. Rob van Veen, *J. Phys. Chem. C* **2012**, 116, 21416-21429.

[22] G. Crépeau, V. Montouillout, A. Vimont, L. Mariey, T. Cseri, F. Maugé, *J. Phys. Chem. B* **2006**, 110, 15172-15185.

[23] M. F. Williams, B. Fonfé, C. Sievers, A. Abrahan, J. A. van Bokhove, A. Jentrys, J.A.R. van Veen, J.A. Lercher, *J. Catal.* **2007**, 251, 485-496.

[24] D. G. Poduval, J. A. Rob van Veen, M. S. Rigutto, E. J. M. Hensen, *Chem. Commun.* **2010**, 46, 3466-3468.

[25] M. Valla, A. J. Rossini, M. Caillot, C. Chizallet, P. Raybaud, M. Digne, A. Chaumonnot, A. Lesage, L. Emsley, J. A. van Bokhoven, C. Copéret, *J. Am. Chem. Soc.* **2015**, 137, 10710-10719.

[26] M. Caillot, A. Chaumonnot, M. Digne, J.A. van Bokhoven, *J. Catal.* **2014**, 316, 47-56.

[27] P. Djinović, T. Tomše, J. Grdadolnik, Š. Božič, B. Erjavec, M. Zabilskiy, A. Pintar, *Catal.Today* **2015**, 258, 648-659.

[28] G. Busca, *Chem. Rev.* **2007**, 107, 5366-5410.

[29] C. Arasa, H.F. Busnengo, A. Salin, R. Sayós, *Surf. Sci.* **2008**, 602, 975-985.

[30] D. Yun, T.Y. Kim, D.S. Park, Y.S. Yun, J.W. Han, J. Yi, *ChemSusChem* **2014**, 7(8), 2198-2201.

[31] A. Kawamoto, K. Cho, P. Griffin, R. Dutton, *J. Appl. Phys.* **2001**, 90, 1333-1341.

[32] T.Y. Kim, J. Baek, C.K. Song, Y.S. Yun, D.S. Park, W. Kim, J.W. Han, J. Yi, *J. Catal.* **2015**, 323, 85-99.

[33] J. Handzlik, R. Grybos, F. Tielens, *J. Phys. Chem. C* **2013**, 117, 8138-8149.

[34] J. Huang, N. van Vegten, Y. Jiang, M. Hunger, A. Baiker, *Angew. Chem. Int. Ed.* **2010**, 49, 7776-7781.

[35] G. Kresse, J. Furthmuller, *Phys. Rev. B: Condens. Matter* **1996**, 54,

11169-11186.

[36] J.P. Perdew, K. Burke, M. Ernzerhof, *Phys. Rev. Lett.* **1996**, 77, 3865–3868.

[37] P. E. Blöchl, *Phys. Rev. B: Condens. Matter* **1994**, 50, 17953-17979.

[38] S. Grimme, *J. Comput. Chem.* **2006**, 27, 1787-1799.

[39] X. Rozanska, F. Delbecq, P. Sautet, *Phys. Chem. Chem. Phys.* **2010**, 12, 14930-14940.

[40] F. Vigné-Maeder, P. Sautet, *J. Phys. Chem. B* **1997**, 101, 8197−8203.

[41] J. Handzlik, J. Ogonowski, *J. Phys. Chem. C* **2012**, 116, 5571-5584.

[42] J. Handzlik, *J. Phys. Chem. C* **2007**, 111, 9337−9348.

[43] R.F.W. Bader, Atoms in Molecules: A Quantum Theory, Oxford University Press, Oxford, **1990**.

[44] C.S. Callam, S.J. Singer, T.L. lowary, C.M. Hadad, *J. Am. Chem. Soc.* **2001**, 123, 11743-11754.

[45] G. Henkelman, H. Jonsson, *J. Chem. Phys.* **2000**, 113, 9978–9985.

[46] G. Henkelman, B.P. Uberuaga, H. Jonsson, *J. Chem. Phys.* **2000**, 113, 9901–9904.

[47] Y. Choi, Y.S. Yun, H. Park, D.S. Park, D. Yun, J. Yi, *Chem. Commun.* **2014**, 57(50), 7652-7655.

[48] P. Sreenivasulu, D. Nandan, M. Kumar, N. Viswanadham, *J. Mater. Chem. A: Chem.* **2013**, 1, 3268-3271.

[49] M.-C. Chao, H.-P. Lin, C.-Y. Mou, B.-W. Cheng, C.-F. Cheng, *Catal. Today* **2004**, 97, 81-87.

[50] C.-F. Cheng, H.-H. Cheng, L.-L. Wu, B.-W. Cheng, *Stud. Surf. Sci. Catal.* **2005**, 156, 113-118.

[51] S. Zhai, Y. Zhang, D. Wu, Y. Sun, S. Wang, *Top Catal.* **2006**, 39, 227-235.

[52] D. Zhou, Y. Bao, M. Yang, N. He, G. Yang, *J. Mol. Catal. A: Chem.* **2006**, 244, 11-19.

[53] M.A.M. Khraishenh, M.A. Al-Ghouti, S.J. Allen, M.N. Ahmad, *Water Res.* **2005**, 39, 922-932.

[54] G. Maccaferri, W. Caminati, P.G. Favero, *J. Chem. Soc. Faraday Trans.* **1997**, 93(23), 4115-4117.

[55] T. Steiner, *Angew. Chem. Int. Ed.* **2002**, 41, 48-76.

[56] X. Wang, Y. Huang, Z. Pan, Y. Wang, C. Liu, *J. Hazard. Mater.* **2015**, 295, 43-54.

[57] E. Yoda, A. Ootawa, *Appl. Catal. A: Gen.* **2009**, 360, 66-70.

[58] C. Michel, F. Auneau, F. Delbecq, P. Sautet, *ACS Catal.* **2011**, 1, 1430-1440.

[59] T. D. Courtney, V. Nikolakis, G. Mpourmpakis, J. G. Chen, D. G. Vlachos, *Appl. Catal A: Gen.* **2012**, 449, 59-68.

[60] J. Yang, S. Meng, L. Xu, E.G. Wang, *Phys. Rev. B* **2005**, 71, 035413.

[61] L.R. Merte, G. Peng, R. Bechstein, F. Rieboldt, C.A. Farberow, L.C.

Grabow, W. Kudernatsch, S. Wendt, E. Lægsgaard, M. Mavrikakis, F. Besenbacher, *Science* **2012**, 336, 889-893.

[62] G.S. Parkinson, Y.K. Kim, Z Dohnálek, R.S. Smith, B.D. Kay, *J. Phys. Chem. C* **2009**, 113, 4960-4969.

[63] K.D. Kwon, V. Vadillo-Rodriguez, B.E. Logan, J.D. Kubicki, Geochim. *Cosmochim. Ac.* **2006**, 70, 3803-3819.

[64] Y.T. Kim, S.J. You, K.D. Jung, E.D. Park, *Bull. Korean Chem. Soc.* **2012**, 33, 2369-2377.

[65] W. Bühler, E. Dinjus, H.J. Ederer, A. Kruse, C. Mas, *J. Supercrit. Fluids* **2002**, 22, 37-53.

[66] E. Tsukuda, S. Sato, R. Takahashi, T. Sodesawa, *Catal. Commun.* **2007**, 8, 1349-1353.

[67] S.H. Chai, H.P. Wang, Y. Liang, B.Q. Xu, *Green Chem.* **2007**, 9, 1130-1136.

[68] S.H. Chai, B. Yan, L.Z. Tao, Y. Liang, B.Q. Xu, *Catal. Today* **2014**, 234, 215-222.

[69] B. Katryniok, S. Paul, V. Bellière-Baca, P. Rey, F. Dumeignil, *Green Chem.* **2010**, 12, 2079-2098.

[70] B. Katryniok, S. Paul, M. Capron, V. Bellière-Baca, P. Rey, F. Dumeignil, *ChemSusChem* **2012**, 5, 1298-1306.

[71] P. Castaño, G. Elordi, M. Olazar, A.T. Aguayo, B. Pawelec, J. Bilbao, *Appl. Catal. B: Environ.* **2011**, 104, 91-100.

[72] B. Guichard, M. Roy-Auberger, E. Devers, B. Rebours, A.A.

Quoineaud, M. Digne, *Appl. Catal. A: Gen.* **2009**, 367, 1-8.

[73] C.E. Snape, B.J. McGhee, S.C. Martin, J.M. Andresen, *Catal. Today* **1997**, 37, 285-293.

[74] M. Rozwadowski, M. Lezanska, J. Wloch, K. Erdmann, R. Golembiewski, J. Kornatowski, *Chem. Mater.* **2001**, 13, 1609-1616.

[75] M. Hunger, *Micropor. Mesopor. Mat.* **2005**, 82, 241-255.

[76] J.L. Bonardet, M.C. Barrage, J. Fraissard, *J. Mol. Catal. A: Chem* **1995**, 96, 123-143.

[77] H. Park, Y.S. Yun, T.Y. Kim, K.R. Lee, J. Baek, J. Yi, *Appl. Catal. B: Environ.* **2015**, 176, 1-10.

[78] J. Barrault, J.-M. Clacens, Y. Pouilloux, *Top. Catal.* **2004**, 27, 137-142.

[79] G. S. Foo, D. Wei, D. S. Sholl, C. Sievers, *ACS Catal.* **2014**, 4, 3180-3192.

[80] F. Wang, J. L. Dubois, W. Ueda, *J. Catal.* **2009**, 268, 260-267.

[81] W. T. Reichle, *J. Catal.* **1980**, 63, 295-306.

[82] F. Leydier, C. Chizallet, A. Chaumonnot, M. Digne, E. Soyer, A.-A. Quoineaud, D. Costa, P. Raybaud, *J. Catal.* **2011**, 284, 215-229.

[83] X. Lin, Y. Lv, Y. Qu, G. Zhang, Y. Xi, D. L. Phillips, C. Liu, *Phys. Chem. Chem. Phys.* **2013**, 15, 20120 –20133.

[84] Y. Toda, H. Hirayama, N. Kuganathan, A. Torrisi, P. V. Sushko, H. Hosono, *Nat. Commun.* **2013**, 4, 10.1038/ncomms3378.

[85] C. J. Jia, Y. Liu, W. Schmidt, A. H. Lu, F. Schth, *J. Catal.* **2010**, 269, 71–79.

[86] T. Q. Hoang, X. Zhu, T. Danuthai, L. L. Lobban, D. E. Resasco, R. G. Mallinson, *Energy Fuels* **2010**, 24, 3804 –3809.

[87] D. S. Park, D. Yun, Y. Choi, T. Y. Kim, S. Oh, J. H. Cho, J. Yi, *Chem. Eng. J.* **2013**, 228, 889 –895.

[88] D. W. Sindorf, G. E. Maciel, *J. Am. Chem. Soc.* **1983**, 105, 1487–1493.

[89] I. S. Chuang, G. E. Maciel, *J. Phys. Chem. B* **1997**, 101, 3052 – 3064.

[90] M. A. Ecormier, K. Wilson, A. F. Lee, *J. Catal.* **2003**, 215, 57–65.

[91] M. Brändle, J. Sauer, *J. Am. Chem. Soc.* **1998**, 120, 1556 – 1570.

[92] F. wang, J. L. Dubois, W. Ueda, *J. Catal.* **2009**, 268, 260 –267.

[93] B. Katryniok, S. Paul, M. Capron, C. Lancelot, V. Bellire-Baca, P. Rey, F. Dumeignil, *Green Chem.* **2010**, 12, 1922 –1925.

[94] P. Lauriol-Garbey, S. Loridant, V. Bellire-Baca, P. Rey, J. M. M. Millet, *Catal. Commun.* **2011**, 16, 170 –174.

[95] D. S. Park, B. K. Kwak, N. D. Kim, J. R. Park, J. H. Cho, S. Oh, J. Yi, *ChemCatChem* **2012**, 4, 836– 843.

[96] F. Cavani, S. Guidetti, C. Trevisanut, E. Ghedini, M. Signoretto, *Appl. Catal. A* **2011**, 409 –410, 267– 278.

[97] M. R. Nimlos, S. J. Blanksby, X. Qian, M. E. Himmel, D. K. Johnson, *J. Phys. Chem. A* **2006**, 110, 6145 –6156.

국 문 초 록

바이오매스 전환 공정은 기존 석유화학산업 기반의 공정보다 친환경적이며, 높은 경제성을 가진다. 바이오매스 전환공정에 효율적이고, 안정적인 촉매를 개발하기 위해서는 먼저 반응 메커니즘을 파악하는 것이 중요하다. 바이오매스 기반 자원인 글리세롤로부터 아크롤레인을 생산하는 탈수반응은, 프로필렌으로부터 아크롤레인을 생산하는 기존 상용공정보다 산업적으로 큰 가치를 창출할 수 있는 반응 경로이다. 그러나 이 반응은 중간생성물이 불안정하여, 촉매 상에서 반응 메커니즘을 실험적으로 관찰하기 힘들다는 한계점을 갖는다.

따라서, 브뢴스테드 산특성을 갖는 비정질 알루미노실리케이트 산촉매 상에서 글리세롤 탈수반응의 메커니즘을 밀도범함수이론(Density functional theory) 계산을 통해 먼저 파악하고자 하였다. 비정질 알루미노실리케이트(amorphous aluminosilicate)는 다양한 산촉매 반응에 높은 활성을 보임에도 불구하고 이에 대한 시뮬레이션 연구가 더디게 진행되고 있는데, 이는 주기성을 갖는 양자역학 이론 계산에서 비정질성을 구현하기가 어렵기 때문이다. 이 연구에서는 이와 같은 한계를 극복하기 위하여, 비정질 실리카와 물리화학적 성질이 비슷하다고 알려진 베타-크리스토발라이트(β-cristobalite) 모델을 기반으로

비정질 알루미노실리케이트 고체산 표면을 구현하였다. 또한 구현된 비정질 알루미노실리케이트 촉매의 브뢴스테드 산점에서 글리세롤 탈수반응 메커니즘을 양자역학 이론 계산을 통해 탐색하였다. 글리세롤의 흡착 구조 및 흡착력, 단계 반응에서의 활성화 에너지를 계산한 결과, 비정질 알루미노실리케이트 고체산에서 글리세롤은 적절한 흡착 세기와 낮은 활성화에너지를 갖는 경로인 아크롤레인으로의 선택적 전환이 가능하다는 것을 확인하였다. 또한, 비정질 알루미노실리케이트 상에 글리세롤이 매우 강하게 흡착될 경우, 글리세롤의 전환이 더디게 일어날 뿐만 아니라, 중합반응을 통해 코크가 촉매표면에 침적됨을 $^{13}C-NMR$ 분석을 통해 증명하였다.

코크침적으로 인한 촉매의 비활성화는 고체산촉매를 사용하는 기상 글리세롤 전환에 해결해야 할 문제로 남아있다. 이를 해결하기 위하여 우리는 브뢴스테드 산 특성을 가지며 열린 기공 구조를 갖는 MS-FS를 제조하여 이 반응에 촉매로 적용하였으며, 약 50시간 동안 높은 수율의 아크롤레인(73%)을 얻을 수 있었다. 계층적인 기공 구조를 갖는 MS-FS촉매는 제올라이트 촉매와 비교하였을 때 더 산화되기 쉬운 코크가 생성된다는 것과, 비슷한 양의 코크침적에도 불구하고 기공 입구가 막히지 않음을 BET, TPO 분석을 통해 확인하였다. 이러한 MS-FS의 기공 구조는 기공 안쪽에 있는 활성점이 긴 반응시간 동안에도 지속적으로 작용할 수 있기 때문에 안정적으로 아크롤레인을 생산하는 데

유리함을 관찰할 수 있었다. 또한 연속적으로 일어나는 두 번의 탈수반응에서 MS-FS 촉매는 산점이 비교적 쉽게 재생되기 때문에 코크 전구체가 생성되는 3-하이드록시프로피온알데히드(3-HPA)의 부반응을 막아 높은 아크롤레인 선택도와 촉매 안정성을 보임을 양자역학 이론 계산을 이용하여 규명할 수 있었다.

주요어: 글리세롤 탈수반응, 아크롤레인, 촉매 안정성, 반응 기작

학 번: 2011-21051

List of publications

International Publications

International Academic Published Papers (First Author)

1. **D. Yun**, Y. S. Yun, T. Y. Kim, H. Park, J. M. Lee, J. W. Han*, and J. Yi* (*co-corresponding author), "Mechanistic Study of Glycerol Dehydration on Brønsted Acidic Amorphous Aluminosilicate", *Journal of Catalysis* 2016, 341, 33-43.

2. **D. Yun***, T. Y. Kim*, D. S. Park, Y. S. Yun, J. W. Han, J. Yi (*co-first author) , "A Tailored Catalyst for the Sustainable Conversion of Glycerol to Acrolein: Mechanistic Aspect of Sequential Dehydration", ChemSusChem 2014, 7(8), 2193-220.

   (*Danim Yun and Tae Yong Kim contributed equally to this work)

3. D. S. Park*, **D. Yun***, T. Y. Kim, J. Baek, Y. S. Yun, and J. Yi (*co-first author), "A Mesoporous Carbon-Supported Pt Nanocatalyst for the Conversion of Lignocellulose to Sugar Alcohols", *ChemSusChem* 2013, 6(12), 2281-2289.

   (*Danim Yun and Dae Sung Park contributed equally to this work)

4. **D. Yun***, J. Baek*, Y. Choi, W. Kim, H. J. Lee, and J. Yi, "Promotional effect of Ni on a CrO_x catalyst supported on silica in the oxidative dehydrogenation of propane using CO_2", *ChemCatChem* 2012, 4(12), 1952-1959.

   (*Danim Yun and Jayeon Baek contributed equally to this work)

International Academic Published Papers (Co-author)

1. Y. S. Yun, T. Y. Kim, **D. Yun**, K. R. Lee, J. W. Han*, and J. Yi* (*co-corresponding author), "Understanding the reaction mechanism of glycerol hydrogenolysis over $CuCr_2O_4$ catalyst", *ChemSusChem*, 2016, 9, 1-14.

2. Y. S. Yun, K. R. Lee, H. Park, T. Y. Kim, **D. Yun**, J. W. Han, and J. Yi, "Rational Design of a Bi-functional Catalyst for the Oxydehydration of Glycerol: A Combined Theoretical and Experimental Study", *ACS Catalysis* 2015, 5, 82-94.

3. Y. Choi*, Y. S. Yun*, H. Park, D. S. Park, **D. Yun**, and J. Yi, "A Facile Approach for Preparation of Tunable Acid Nano-Catalyst with Hierarchically Mesoporous Structure", *Chemical Communications* 2014, 57(50), 7652-7655.

4. D. S. Park, **D. Yun**, Y. Choi, T. Y. Kim, S. Oh, J.-H. Cho, and J. Yi, "Effect of 3D open-pores on the dehydration of n-butanol to di-n-butyl ether (DNBE) over a supported heteropolyacid catalyst", *Chemical Engineering Journal*, 2013, 228, 889-895.

5. Y. Choi, D. S. Park, H. J. Yun, J. Baek, **D. Yun**, and J. Yi, "Mesoporous Siliconiobium Phosphate as a Pure Brønsted Acidic Catalyst with Excellent Performance for the Dehydration of Glycerol to Acrolein", *ChemSusChem*, 2012, 5(12), 2460-2468.

6. J. Baek, H. J. Yun, **D. Yun**, Y. Choi, and J. Yi, "Preparation of highly dispersed chromium oxide catalysts supported on mesoporous silica for the oxidative dehydrogenation of propane using CO2: Insight into the nature of catalytically active chromium sites", *ACS Catalysis*, 2012, 2(9), 1893-1903.

Patents Application on File

1. 이종협, 최영보, 윤양식, 박홍석, **윤다님**, "3차원의 열린 기공 구조를 갖는 알루미노실리케이트 구형 나노 입자, 그 제조방법 및 상기 나노 입자를 이용하여 글리세롤로부터 아크릴산을 제조하는 방법" 특허 제 10-1337301호 (2013.11.29) (특허 출원 10-2012-0031597호, 2012.03.28)
2. 이종협, **윤다님**, 이경록, 박대성, "에너지 절약형 촉매 반응기" 특허 출원 10-2016-0073637 (2016.06.14)
3. 이종협, 박대성, **윤다님**, 윤양식, 박홍석, "금속이 분산된 열린 기공구조를

가지는 탄소 촉매 및 이를 이용한 소르비톨의 생산방법" 특허 제 10-1535123호 (2015.07.02) (특허 출원 10-2014-0001636, 2014.01.07)

International Conferences (First author)

1. **D. Yun**, T. Y. Kim, Y. S. Yun, J. M. Lee, J. W. Han, and J. Yi, "Ab initio study of the surface model of amorphous aluminosilicate", *The 15th Korea-Japan Symposium on Catalysis*, BEXCO and Haeundae Centum Hotel, Busan, Korea, May. 26-28, 2015.
2. **D. Yun**, D. S. Park, T. Y. Kim, S. Oh, Y. A. Shin, and J. Yi, "Preparation of DSS-SO_3H Catalyst for Stable Production of Acrolein from Glycerol" *The 14th Japan-Korea Symposium on Catalysis*, WINC Aichi, Nagoya, Japan, July 1-3, 2013.

International Conferences (Co-author)

1. H. Park, Y. S. Yun, **D. Yun**, T. Y. Kim, K. R. Lee, J. Baek, M. Lee, and J. Yi, "An investigation of deactivation mechanism by coke via kinetics study of the glycerol dehydration over acid catalysts", *16th International Congress on Catalysis*, CNCC, Beijing, China, July. 3-8, 2016
2. Y. S. Yun, K. R. Lee, H. Park, T. Y. Kim, **D. Yun**, J. W. Han, and J. Yi, "Bi-Functional Mo-V-W-O Catalysts for the One-Step Production of Acrylic Acid from Glycerol and Validation Via First Principle Calculations", *24th North American Catalysis Society Meeting,* David L. Lawrence Convetion Center, Pittsburgh, Pennsylvania, USA, June. 14-19, 2015
3. Y. S. Yun, T. Y. Kim, **D. Yun**, H. Park, J. M. Lee, J. W. Han, and J. Yi, "Mechanistic insight of hydrogenolysis of glycerol over Cu-based catalysts via ab initio calculations", The 15th Korea-Japan Symposium on Catalysis, Busan, Korea, May. 26-28, 2015.

4. D. S. Park, **D. Yun**, Y. S. Yun, H. Park, T. Y. Kim, J. Baek, J. Yi, "Direct conversion of lignocellulose to sugar alcohols over Pt supported on a new 3D mesoporous carbon", 247th American Chemical Society National Meeting & Exposition, Dallas, Texas, USA, Mar. 16-20, 2014.

5. Y. S. Yun, Y. Choi, H. Park, **D. Yun**, D. S. Park, and J. Yi, "Preparation of 3D Open-Porous Acidic Heterogeneous Catalysts for the Chemical Production", *2013 MRS Fall Meeting Program & Exhibit*, Boston, Massachusetts, USA, Dec. 1-6, 2013.

6. D. S. Park, **D. Yun**, Y. Choi, T. Y. Kim, S. Oh, J.-H. Cho, and J. Yi, "Enhancement of Mass Transport over 3D Open-porous Dandelion-like Catalyst in Liquid-phase Heterogeneous Catalysis", 9th World Congress of Chemical Engineering, Coex, Seoul, Korea, August 18-23, 2013.

7. Y. S. Yun, Y. Choi, H. Park, **D. Yun**, and J. Yi, "Three dimensionally open porous acid catalysts with adjustable acidic properties", *The 14th Japan-Korea Symposium on Catalysis*, WINC Aichi, Nagoya, Japan, July 1-3, 2013.

8. D. S. Park, Y. S. Yun, **D. Yun**, S. Oh, Y. A. Shin, and J. Yi, "The hydrogenolysis of glycerol on CuNi bimetallic catalyst supported on mesoporous alumina", *The 14th Japan-Korea Symposium on Catalysis*, WINC Aichi, Nagoya, Japan, July 1-3, 2013.

Domestic Conferences

1. **윤다님**, 윤양식, 김태용, 박홍석, 한정우, 이종협, "비정질 알루미노실리케이트 촉매의 브뢴스테드 산 점에서 글리세롤 탈수반응 메커니즘 연구", 추계 한국화학공학회, 대전컨벤션센터, 10. 19-21 (2016)
2. 송찬경, 백자연, 유성주, 김태용, **윤다님**, 박홍석, 이경록, 이종협, "TiO_2 상과 구조적 효과에 의한 가시광선 영역에서 Au/TiO_2의 광촉매 활성 분석", 한국화학공학회 2016년도 봄 총회 및 학술대회, 부산 BEXCO, 4. 27-29 (2016)

3. 윤양식, 이경록, 박홍석, 김태용, **윤다님**, 서영종, 김왕규, 이중원, 한정우, 이종협, “글리세롤의 산화탈수반응을 위한 이원기능촉매 개발 및 적용”, 추계 한국화학공학회, 대전컨벤션센터, 10. 23-24 (2014)
4. 박대성, **윤다님**, 이종협, 오석일, 신용안, “3차원 구조의 중형기공 탄소물질의 제조 및 리그노셀룰로오스 직접전환을 통한 당알코올 생산에의 응용”, 한국화학공학회 2014년도 봄 총회 및 학술대회, 창원컨벤션센터, 4. 23-25 (2014)
5. **윤다님**, 김태용, 박대성, 윤양식, 이종협, 한정우, 오석일, 신용안, “글리세롤로부터 아크롤레인을 안정적으로 생산하기 위한 맞춤형 촉매 개발’, 춘계 한국화학공학회, 창원컨벤션센터, 4. 23-25 (2014)
6. **윤다님**, 김태용, 박대성, 윤양식, 한정우, 이종협, “열린 기공 구조를 갖는 브뢴스테드 산촉매의 제조 및 글리세롤 탈수반응에의 적용’, 춘계 한국청정기술학회, 여수경도리조트, 3. 27-28 (2014)
7. 윤양식, 박홍석, **윤다님**, 박대성, 김태용, 백자연, 이경록, 이종협, “계층구조를 갖는 나노크기의 고체산촉매 제조 및 응용”, 춘계 한국청정기술학회, 여수경도리조트, 3. 27-28 (2014)
8. 박대성, **윤다님**, 윤양식, 김우식, 이종협, “3차원 중형기공 탄소물질의 개발 및 목질계 바이오매스 전환을 통한 당알코올 생산기술에의 응용”, 한국청정기술학회 춘계 학술발표회, 여수경도리조트, 3. 27-28 (2014)
9. 백자연, 송현돈, 김태용, 박대성, **윤다님**, 윤양식, 박홍석, 이종협, “금 나노입자의 암모니아 보란을 이용한 4-니트로페놀 환원 반응에서의 실시간 전자이동 관찰”, 추계 한국청정기술학회, 제주한화리조트, 9. 25-27 (2013)
10. 윤양식, 박대성, **윤다님**, 김태용, 오석일, 이종협, “무수소 조건에서의 글리세롤의 가수소분해 반응을 위한 중형기공 알루미나에 담지된 구리-니켈 이중금속촉매의 제조 및 적용’, 춘계 한국청정기술학회, 여수 경도리조트, 3. 28-29 (2013)
11. 박대성, **윤다님**, 오석일, 신용안, 이종협, “3차원 다공성촉매를 이용한 n-butanol의 탈수반응 및 속도론적 해석을 통한 내부확산의 영향” 2013년 한국청정기술학회 춘계 학술발표회, 여수 경도리조트, 3. 28-29 (2013)
12. 백자연, **윤다님**, 최영보, 김태용, 김우영, 이희종, 김영훈, 이종협, “이산화

탄소/프로판을 원료로 사용하는 프로필렌 제조용 촉매 공정 개발 1. 고효율 촉매 설계 및 제조", 추계 한국청정기술학회, 영남대학교, 11. 16 (2012)

13. 박대성, **윤다님**, 오석일, 조정희, 이종협, "바이오매스 유래 글리세롤의 고부가가치용 촉매 공정 개발 2. Coking 최소화 촉매 개발", 2012년 추계 한국청정기술학회, 영남대학교, 11. 16 (2012)
14. **윤다님**, 백자연, 최영보, 김우영, 이희종, 김영훈, 이종협, "이산화탄소/프로판을 원료로 사용하는 프로필렌 제조용 촉매 공정 개발 2.안정성 최대화 촉매 개발", 2012년 추계 한국청정기술학회, 영남대학교, 11. 16 (2012)
15. 최영보, 박대성, 백자연, **윤다님**, 이종협, "바이오매스 유래 글리세롤의 고부가가치용 촉매 개발 1.고효율 촉매 설계 및 제조", 2012년 추계 한국청정기술학회, 영남대학교, 11. 16 (2012)
16. **윤다님**, 백자연, 최영보, 김우영, 이희종, 이종협, "이산화탄소와 프로판으로부터 프로펼렌 제조를 위한 CrOx/SBA-15 촉매의 니켈 첨가에 의한 영향", 한국화학공학회 2012년 가을 학술대회, 부산 BEXCO, 10. 24-26 (2012)
17. 백자연, **윤다님**, 윤형진, 최영보, 김우영, 이희종, 이종협, "중형기공실리카에 크롬산화물이 고분산된 Cr-MSU-x 촉매의 제조 및 이산화탄소를 산화제로 사용한 프로판의 산화 탈수소화 반응(ODHP)에서의 촉매특성연구", 한국화학공학회 2012년 가을 학술대회, 부산 BEXCO, 10. 24-26 (2012)
18. 윤양식, 최영보, **윤다님**, 박홍석, 이종협, "글리세롤의 산화탈수반응을 위한 다공성 산성 나노촉매의 제조 및 분석", 한국화학공학회 봄 총회 및 학술대회, 제주국제컨벤션센터, 4.25-27 (2012)
19. 백자연, **윤다님**, 윤형진, 최영보, 김우영, 이희종, 이종협, "이산화탄소를 산화제로 사용한 프로판의 산화 탈수소화 반응(ODHP)에서의 Cr-MSU-x 촉매 특성연구", 추계 한국화학공학회, 송도컨벤시아, 10. 26-28 (2011)
20. 최영보, 박대성, 윤형진, 백자연, **윤다님**, 이종협, "새로운 산촉매 개발과 글리세롤 탈수 반응에의 적용", 추계 한국화학공학회, 송도컨벤시아, 10. 26-28 (2011)